UNIONE EUROPEA
Fondo Sociale Europeo

Ministero dell'Università e della Ricerca

PON RICERCA E INNOVAZIONE 2014 - 2020

UNIVERSITÀ DEGLI STUDI FIRENZE
Da un secolo, oltre.

DOTTORATO DI RICERCA IN
ATOMIC AND MOLECULAR PHOTONICS

CICLO XXXVII - PON ex DM1061

Development and testing of porous materials for metal recovery from wastewater

Settore Scientifico Disciplinare: FIS / 03

Dottoral Candidate
Dott.ssa *Pamela Cinfrignini*

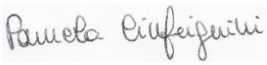

Supervisor
Prof. *Renato Torre*

Co-Supervisor
Dr. *Daniele Martella*

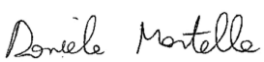

Coordinator
Prof. *Diederik Sybolt Wiersma*

Years 2022 - 2024

Alla mia famiglia.

L'albatros

Souvent, pour s'amuser, les hommes d'équipage
Prennent des albatros, vastes oiseaux des mers,
Qui suivent, indolents compagnons de voyage,
Le navire glissant sur les gouffres amers.

A peine les ont-ils déposés sur les planches,
Que ces rois de l'azur, maladroits et honteux,
Laissent piteusement leurs grandes ailes blanches
Comme des avirons traîner à côté d'eux.

Ce voyageur ailé, comme il est gauche et veule!
Lui, naguère si beau, qu'il est comique et laid!
L'un agace son bec avec un brûle-gueule,
L'autre mime, en boitant, l'infirme qui volait!

Le Poète est semblable au prince des nuées
Qui hante la tempête et se rit de l'archer;
Exilé sur le sol au milieu des huées,
*Ses ailes de géant l'empêchent de marcher***.**

Charles Baudelaire

Index

1. Introduction

This thesis encompasses the experimental work conducted over the past three years, focusing on the development, characterization, and optimization of porous materials for the selective recovery of precious metals from industrial wastewater.

The recovery of noble metals from industrial wastewater and electronic waste has become increasingly critical to ensure the sustainable use of these non-renewable resources. Industries such as jewellery manufacturing and electronics contribute significantly to the demand for metals such as gold, platinum, and palladium, while simultaneously generating waste streams that contain trace amounts of these valuable elements. Efficient recovery techniques are essential not only for economic reasons but also to mitigate environmental impacts.

Gold, a noble metal with a wide range of applications, has played a significant role in human development. Historically used as a monetary material and bank reserve (retaining its financial value to this day), it continues to meet high demand across various industries, from jewellery to technological devices and central banks. In 2023, the global demand for gold exceeded 4.4 ktons, with 3.6 ktons of this supply coming from mining and the rest from recycling processes.

(**Figure 1a**) [1]. Due to its relative scarcity compared to common base metals and the growing needs of modern society, gold recycling has become an essential aspect of industrial processes and urban waste management. Various strategies have been developed for gold extraction, not only from ores but also from secondary sources, which form an "urban mine" of electronic waste or end-of-life catalysts. These sources often contain noble metals at concentrations higher than those found in natural ores [2]. For instance, gold is commonly found in printed circuit boards with concentrations of up to 3.6 g Kg^{-1} [2]. Other important sources for gold recycling are also the wastewater of different metal industries, where such elements are mixed with a very complex composition and concentration below 20 mg L^{-1}.

Gold extraction methods can vary, but a major challenge is the separation of gold from other precious metals that coexist in multi-metal catalysts, electronic devices, and wastewater. Focusing on gold separation from other metals, hydro and solvo-metallurgic processes can be considered as the most versatile and promising ones for the selective recovery that can be obtained by different chemical processes shown in **Figure 1b.** For all these methodologies, a complete overview over recent developments and their sustainability is reported in previous review works, [3,4] while the examples cited above just show the potentiality of the different pathways. Indeed, selective gold dissolution can be introduced by appropriate choice of the oxidant (e.g. in ethanol using 2-mercaptobenzimidazole - 2-MBI- as ligand and iodine) [5] or exploiting a kinetic control, e.g. during time-dependent photocatalytic dissolution (with TiO_2 nanoparticles under UV light) [6]. On the other hand, all metals can be dissolved together and then separated in solution by additional steps. These should include separation by ion-exchange resins, selective precipitation (e.g. by cyclodextrin), [7] selective reduction (e.g. with chloride leaching followed by oxalic acid

reduction) [8] or selective extraction in organic solvent (e.g. by different amides) [9]. These methods, however, often require large amounts of organic solvents or hazardous chemicals and generate waste that must be carefully managed. Moreover, these processes can be time-consuming, involving multiple steps. An alternative solution is provided by a range of absorbent materials, such as carbon materials, hydrogels, biopolymers, silicas, and metal-organic frameworks (MOFs) [10,11]. Some materials, including food waste derivatives, have proven to be a sustainable solution for separating gold from leaching solutions of e-waste, efficiently removing gold from base metals and others [12]. However, selectivity towards platinum group metals remains poorly addressed. The separation of gold from Pd, Pt, Ir, and Rh, which share similar properties, remains a significant challenge.

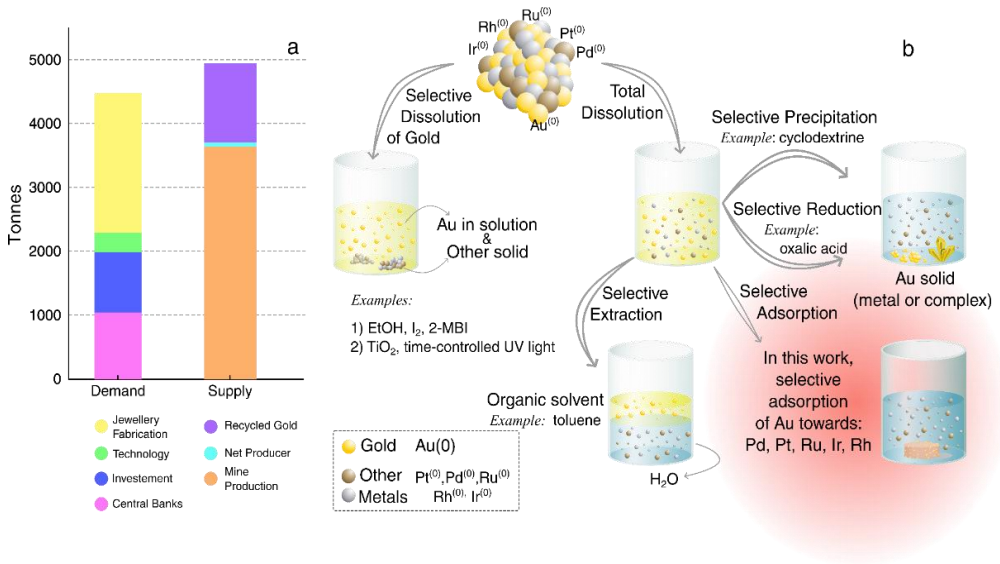

Figure 1: Need of gold in 2023 (a) and possible strategies for its separation by other precious metals recycling of this metal (b). Strategies reported in panel b represent the key steps for metal recycling and will be crucial over the next years for the sustainability of gold supply.

Currently, simultaneous recovery of gold with Pd and Pt is a bottleneck in selective adsorption. For instance, materials based on polyethyleneimine (PEI) have been described for rapid adsorption (with equilibrium times under 10 minutes), but without selectivity between gold, palladium, and platinum [13, 14]. Other synthetic materials that allows separation of these 3 metals with respect to others (but not in between Au, Pd, and Pt) include poly(ionic liquid)-derived porous organic polycarbene adsorbent [15], or 2-mercaptobenzothiazole-bonded silica gel [16] or aminopropyl silica gel [17]. Similarly, natural materials such as crosslinked chitosan modified with l-lysine [18], chitosan-keratin cryogels modified with vinyl pyrrolidone [19], and amyloid-like protein membranes [20] have shown similar performances. Among the various methods employed for metal recovery, adsorption is particularly valued for its cost-effectiveness, simplicity, and environmentally friendly nature. This process involves mechanisms such as chemisorption, ion exchange, and diffusion through porous structures, which makes it highly versatile. However, despite the development of various adsorbent materials, including nanosized adsorbents with high adsorption capacities, their practical application is often limited by challenges such as difficult recovery, water contamination risks, and high costs [21, 22]. A promising alternative to these conventional adsorbents is hydrogel-based materials, which have gained attention for their potential in efficient metal recovery [23].

In this work, we propose the use of Poly(Acrylamide-co-Acrylic Acid) hydrogels and cryogels containing 2-Hydroxyethyl Acrylate (HEA) and acrylic acid for the selective recovery of gold from complex mixtures containing noble metals such as Pd, Pt, Rh, Ru, and Ir. Specifically, hydrogels based on acrylamide and acrylic acid have demonstrated excellent selectivity for Pt(IV), Rh(III), and Ir(III), and good selectivity for Pd(II) and Ru(III), as discussed in

Chapter 2 [24]. The hydrogels were evaluated for their swelling behaviour, adsorption capacity, and selectivity under various conditions including the acidic pH typical of industrial effluents using standard UV-VIS spectroscopy. Scanning Electron Microscopy (SEM) and Polarized Optical Microscopy (POM) were used to analyze their microstructure and the formation of gold nanoparticles and microplates. Batch tests were conducted to assess the adsorption kinetics of the hydrogels, and various models were explored to describe its temporal evolution. Cryogels were also investigated for their enhanced performance in adsorption applications. Cryogels are porous three-dimensional architectures synthesised via cryopolymerization at subzero temperatures, where the frozen solvent creates a sponge-like structure with interconnected macropores. This structure acts as a porogen, enabling high permeability [25]. Like hydrogels, cryogels rely on acrylic acid as a primary monomer, but they feature additional versatility due to their ability to incorporate either acrylamide or 2-hydroxyethyl acrylate (HEA) as the co-monomer. This structural adjustment investigated in **Chapter 3** enhances the cryogels adsorption efficiency and mechanical properties. Among the tested formulations, cryogels containing HEA alongside acrylic acid demonstrated superior performance, highlighting their potential as advanced materials for selective adsorption. Similarly, the primary techniques utilized in Chapter 2 were employed to assess adsorption performance. Additionally, tests for a more specific material characterization were conducted and Energy Dispersive Spectroscopy (EDS) was employed to gain further insights and confirm the selectivity. Notably, both hydrogels and cryogels do not require any post-treatment or extensive pretreatment of wastewater, such as pH adjustments or the addition of reducing agents, which makes them both simple and industrially applicable. The cryogels, characterized by their interconnected macroporous structure, overcome the limitations of conventional hydrogels by enabling faster diffusion and higher adsorption efficiency.

The study investigates various aspects of porous materials, focusing on the mechanisms of metal adsorption and the influence of composition and synthesis methods on the process. It deepens the functioning of porous materials as adsorbents, examining the absorption and diffusion processes that are fundamental to understanding the underlying physicochemical phenomena. The findings provide important insights into the mechanisms driving metal ion adsorption. However, to our knowledge, no comprehensive physical model exists that can fully explain the complex interactions governing diffusion and adsorption processes.

This research was conducted across the laboratories of European Laboratory for Non-Linear Spectroscopy - LENS (Sesto Fiorentino, Italy), with Prof Renato Torre and Dr. Daniele Martella, the LiPhy Institute (Grenoble, France), in collaboration with the research group headed by Prof. Marie Plazanet, and in cooperation with the company CABRO S.p.A. (Arezzo, Italy), which provided batch samples of industrial wastewater containing precious metals and specific analysis laboratory techniques as Thermogravimetric analysis (TGA) and Inductively Coupled Plasma Optical Emission Spectroscopy (ICP-OES) analysis.

2. Poly(Acrylamide-co-Acrylic Acid) hydrogel as gold adsorbents

2.1. INTRODUCTION

Due to its outstanding physical and chemical attributes such as ductility, conductivity, and catalytic properties, gold is heavily employed in many fields, including industrial manufacturing, electronics, and medicine [26]. In 2023, the demand for gold exceeded its previous record, reaching 4.4 kilotons, excluding OTC (over the counter), with the jewellery industry accounting for nearly 49% of global gold demand [1,27]. The increasing demand for gold is also accompanied by the urgent need of simple methods for its recovery and recycling, due to the non-renewable nature of the material. Of particular interest is the selective recovery of gold from waste sources including electronic waste and industrial wastewater. In the waste solution, a given metal is often present in a mixture with other metals. For industrial processes like gold plating and extraction, the concentration of gold in waste liquids is typically low, sometimes down to trace amounts. Moreover, these waste waters contain various metal ions or salts, which further complicates the recovery of gold. [20] Currently the gold recovery methods widely employed by industries for metal mixtures involve

leaching solutions with multiple cycles of dissolution and activate carbons or ion exchange resins [21]. This last kind of resins has seen an increased employment due to their good versatility, improved gold recoveries from preg-robbing ores, better selectivity for gold over base metals, and moreover, simple and energy-efficient elution/regeneration [22,28]. Indeed, resins are stripped at relatively low temperatures of around 60 °C, while activated carbon is eluted at 120-130 °C [29]. However, gold recovery following the elution process, as well as selectivity, still need substantial enhancements. Other drawbacks include the high costs of materials and energy expenses for combustion.

At the moment, adsorption is considered one of the most promising methods for its low cost, easy operation, as well as environment-friendly characteristics [23]. The mechanism of adsorption broadly includes chemisorption, complexation, adsorption on surface, diffusion through pores and ion exchange. In the last decade, numerous nano-sized adsorbents (including core-shell nanoparticles or nanoflakes) [30] have been prepared exhibiting good performances in terms of adsorption capacity and selectivity. However, the nanosized dimension makes the recovery of the adsorbents itself extremely tricky, especially in large scale processes, resulting in potential water pollution and increased costs for wastewater remediations.

In between different organic adsorbents [31-33], hydrogel-based ones have been considered as potential alternatives; these materials are formed by three-dimensional polymeric networks that can absorb significant amounts of water while remaining insoluble due to chemical or physical cross-linking. Hydrogels can offer a good modulation of the absorption capacity and selectivity by manipulating the functional groups and the structure porosity thus enhancing available specific surface area [34]. For what concerns the gold recovery, both synthetic [35,36] and natural based hydrogels have been reported [37,38]. In the last class, materials obtained from protein waste (e.g. amyloid nanofibrils

[20,39], persimmon peel [40] or hairs [41]) are the most studied towards circular economy, and selective recovery has been demonstrated with respect to many metals, including Cu, Ni, Pb, Zn, Cr, Fe and Mn [39]. Less studied is the selectivity with other precious metals (such as Pt, Rh, Ir, Pd, Ru) that, on the other hand, are still present in industrial wastewater. As an example, lysozyme-based membranes demonstrated an outstanding adsorption capacity for gold but no selectivity when the other platinum group precious metal ions are present in solution [20].

In this study, we propose the use of hydrogel based on a crosslinked copolymer prepared by acrylamide and acrylic acid for the gold recovery. These materials are easy-to-make thus allowing for easy scale up of their standardized preparation; the synthesis employs only low-cost commercial monomers and a classical free radical polymerization thus allowing a scalable and reproducible procedure. Indeed the Poly(acrylamide-co-acrylic acid) hydrogels have been already studied for water treatment, in particular for the adsorption of different cationic dyes (e.g. Methylene Blue, Methyl violet) and metals (including Fe(III), Cr(III), Hg(II), Pb(II), Cu(II), Cd(II)) with main examples reported in **Table 1**. The pH plays a crucial role due to protonation/deprotonation of the functional groups and thus the adsorption performances. Metals are generally adsorbed with pH above 5, while recovery in acid solution has been barely demonstrated. To the best of our knowledge, gold recovery had never been described with this kind of hydrogels. In the last part of the chapter, we demonstrate the gold recovery during a batch adsorption test on an industrial wastewater, with different metal ions competing being present. The metal concentration was lower than 20 ppm, thus more difficult to treat with state-of-the-art methods. During the water treatment, the hydrogel allows a complete selectivity of gold recovery toward Pt^{4+}, Rh^{3+} and Ir^{3+} and a good selectivity with respect to Pd^{2+}, Ru^{3+}. The overall characterization demonstrates the system as promising adsorbent for the

treatment of acid wastewater containing a complex mix of metal cations, such as those obtained by jewellery industries or by electronic waste dissolution.

Table 1. Example of Poly(acrylamide-co-acrylic acid) hydrogel for water treatment.

Adsorbed species	**Other Additives [a]**	**Main features**	**Ref.**
Methylene Blue	Calcium Hydroxide Nanoparticles	Q_e[b] = 1056 mg g^{-1} (at pH=7)	42
Methyl Violet	Attapulgite	Q_e = 1194 mg g^{-1}, Constant performance in the whole pH range 4.5 to 9.8	43
Methylene Blue Methyl Orange Pb(II)	/	Q_e and adsorption rate increase more than ten time with high entangled network	44
Cu(II)	/	Q_e = 121 mg g^{-1} (at pH = 3)	45
Fe(III), Cr(III), Hg(II)	/	Test on single metal solution; Fe(III): Q_e = 276 mg g^{-1} Cr(III): Q_e = 139 mg g^{-1} Optimal pH > 5	46
Pb(II), Cd(II)	Zeolites	Recovery of up to 99% for both metal (for pH above 5 in single ion solution)	47
Pb(II), Cu(II) , Cd(II)	Microcrystalline Cellulose	pH=5 more suitable for metal recovery (test on single ion solution); Cu(II) : Q_e = 177 mg g^{-1} Pb(II): Q_e = 557 mg g^{-1} Cd(II): Q_e = 306 mg g^{-1}	48

Au(III)	-	Q_e = 124 mg g^{-1} (pH=1). Competition test with other metals (Pt(IV), Rh(III), Ir(III), Pd(II), Ru(III))	24 This work

[a] Compounds contained beyond Poly(acrylamide - co - acrylic acid). [b] Q_e being the adsorption capacity at equilibrium calculated considering the equilibrium gold concentration C_e as $C_{t=250h}$ in the Equation (1).

2.2. RESULTS AND DISCUSSION

2.2.1. Material design and preparation

The choice for the hydrogel chemical structures has been based on recent studies that demonstrate how both acrylamide and acrylic acid can be used as a reducing agent for gold cation in solution to obtain gold nanoparticle [49]. Acrylamide can effectively stabilize gold colloids, [50] or it can be polymerized *in-situ* to obtain composite hydrogels with homogeneously distributed nanoparticles [51,52].

In this case, the proposed mechanism involved a direct redox reaction between $HAuCl_4$ and the amide group, with the prior formation of protonated acrylamide and $[AuCl_4]^-$ counterion, which facilitates electron transfer to the amine group [52]. Polyacrylic acid can act simultaneously as a reducing agent and gold nanoparticle stabilizer, resulting in a stable colloidal formulation [53]. Although in all these examples heating between 50 and 80 °C is typically required to accelerate gold reduction, [49-52] here we demonstrate that copolymers of acrylamide and acrylic acid can promote the nanoparticle formation also at room temperature.

The hydrogels, later referred to as Poly(AAm-co-AAc), were prepared by free radical polymerization in an aqueous mixture containing acrylamide (AAm) as the main monomer, acrylic acid (AAc) as comonomer, and N,N'-Methylenebisacrylamide (BIS) as crosslinker [54]. The material preparation is depicted in **Figure 2**. Three different monomer formulations were prepared and, after the addition of ammonium persulfate (APS, as an initiator) and tetramethyl-ethylenediamine (TEMED, as a co-initiator), the polymerization occurred [55]. In all cases, the monomer concentration was fixed at 2 M (in water), and the concentration of BIS was 20 mM. The hydrogels are indicated as to PAAx, where x is the molar concentration of acrylamide, and the different compositions are reported in **Table 2**. For instance, the material labelled PAA1.6 contains acrylamide with a concentration of 1.6 M and 0.4 M acrylic acid.

The ratio between the two co-monomers was adjusted to investigate the potential impact of molecular composition on absorption capabilities and kinetics. Indeed, this parameter is also expected to modulate other physical chemical properties, such as the swelling degree. The efficiency of the polymerization process has been controlled by gel fraction measurements reported in **Table 2**. The hydrogel containing the lower amount of acrylic acid (PAA1.6), presented an almost quantitative polymerization at room temperature, while for the others, heating at 60 °C was employed to obtain a high gel fraction (93%).

Table 2. Different compositions of Poly(AAm-co-AAc) hydrogels and their gel fraction.

	AAm (M)	**AAc** (M)	**BIS** (mM)	**Gel Fraction** (%)
PAA1.6	1.6	0.4	20	99

PAA1	1	1	20	93
PAA0.8	0.8	1.2	20	93

Such materials can be used directly as adsorbents without the need for further chemical treatment. As depicted in **Figure 2**, various wastewater streams containing cationic metals could be treated by simple immersion of the hydrogel in the acid water bath. The treated wastewater should have originated from both industrial waste and the dissolution of metals from electronic waste, among other examples. As introduced in Chapter 1, special emphasis is placed on the selective recovery of one metal over another, enabling the potential recycling of pure species

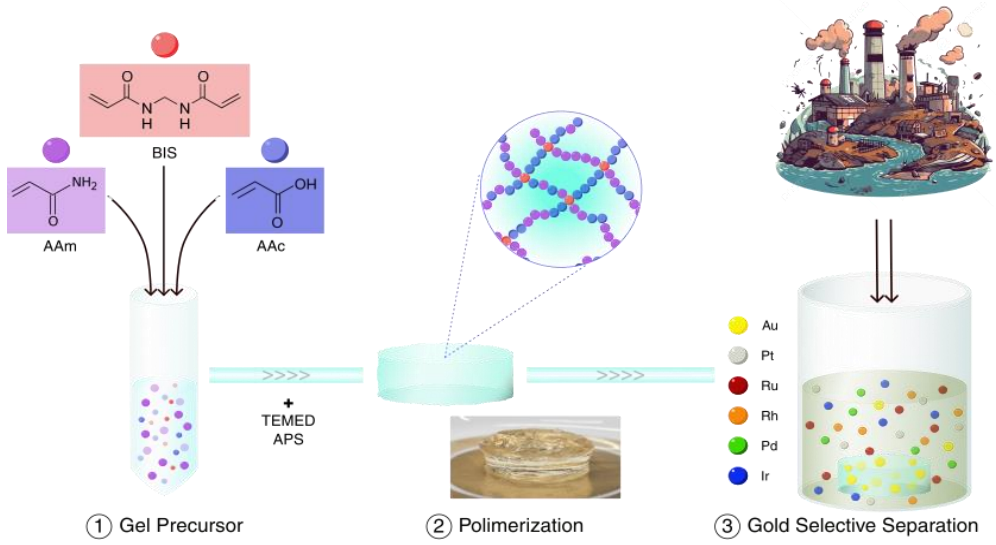

Figure 2. Scheme of the preparation of Poly(AAm-co-AAc) hydrogels and their use for gold recovery. The selective gold adsorption could be conducted in different industrial wastewaters containing competing cations.

The metal recovery performances of a hydrogel (e.g. amount of metals, adsorption kinetic of and selectivity of specific metal with respect to the others), can be determined by the chemical groups available for the adsorption or metal reduction that in turn also influence its structure and swelling capability. In particular, the swelling behaviour of Poly(AAm-co-AAc) hydrogel is strongly influenced by environmental parameters, such as temperature, ionic strength and pH of the solution [56,57]. The water absorption capabilities of each Poly(AAm-co-AAc) hydrogels are reported in **Figure 3** both at neutral and acid pH. The latter was selected since the industrial wastestream analyzed later presented a pH=1. Solution at the same pH is also generally used when the metal cation solutions are obtained by e-waste dissolution [39], thus we believe to represent the more relevant case for gold recovery. The swelling capacity was evaluated by gravimetric methods taking into account the maximum water content incorporated starting from the dry material at the equilibrium, maintaining temperature and ionic strength of the buffer solution constant.

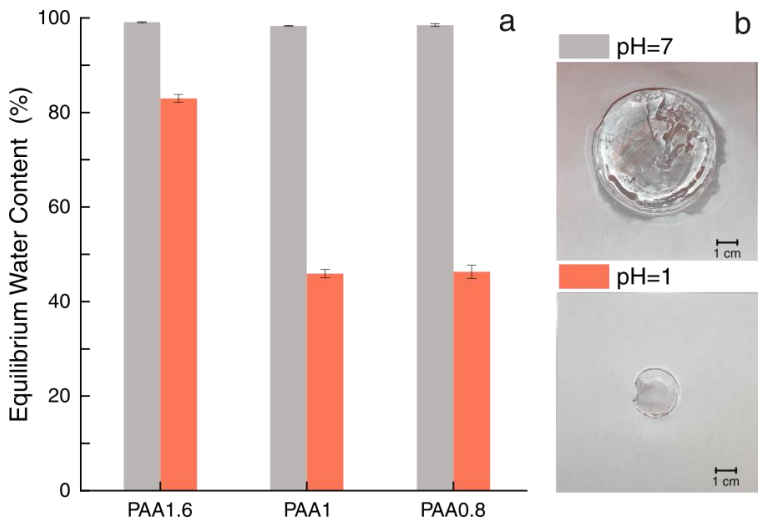

Figure 3. Swelling behaviour of Poly(AAm-co-AAc) hydrogels. Equilibrium Water Content of the hydrogels at different pH (grey bar: pH=7, red bar: pH=1) (a); images of

PAA1.6 treated in deionized water (pH=7) and 0.2M HCl solution (pH=1) respectively (b).

As expected, for all the materials, the equilibrium water content was greatly reduced by lowering the pH from 7 to 1. As an example, in PAA1.6, a reduction from 99% to 83% of the water content was observed as an effect of the carboxylic acid protonation. When pH ≤ pKa, the carboxylic acid groups are not deprotonated (with the acrylic acid dissociation constant pKa= 4.5) [58], and a lower equilibrium water content was observed. Increasing the amount of AAc content, a strong decrease in equilibrium water content at pH=1 was observed between PAA1.6 and PAA1 (83% and 45% respectively) while further addition of AAc led only to small variation of water content. On the other hand, at pH=7 (≥ pKa), the swelling capacity remains almost unchanged with increasing the acrylic acid content [59].

2.2.2. Metal ions adsorption in pure gold solutions.

A detailed characterization of gold adsorption capability and its kinetics by Poly(AAm-co-AAc) hydrogels was conducted using aqueous solutions of Au(III) cations, obtained by dissolving $HAuCl_4$ salts in water (pH = 1). The hydrogel was used for batch adsorption tests, where a specified amount of material was immersed in gold salt solutions at various concentrations (20, 40, 60, and 87 mg L^{-1}). The residual gold salt concentration in solution was monitored using UV-Visible spectroscopy over an extended period, ranging from hours to days, as shown in **Figure 4** for the hydrogel PAA1.6. In particular, UV-Vis absorbance measurements of the solution were monitored every hour (**Figure 4a**). The spectra display two distinct absorption bands in the UV spectral region. At pH < 4, Au (III) chloride exists in the planar $[AuCl_4]^-$ form [60], giving rise to absorption bands at 229 nm and 315 nm as already reported from

aqua regia solutions of $AuCl_4^-$ [61]. In our study, the lower energy peak, corresponding to ligand-metal charge transfer, was chosen to monitor the changes in concentration of the $AuCl_4^-$ ion during its adsorption on the hydrogel. The absorbance variation was used to determine the final concentration according to Lambert-Beer law, using $\varepsilon_{314nm} = (0.01209 \pm 0.00008)$ L $cm^{-1}mg^{-1}$ as the molar absorption coefficient of the gold salt (estimated by the calibration curve reported in **Figure 20**). In **Figure 4b**, the decay of gold concentration as a function of time is reported for 250 h starting from the immersion of the PAA1.6 hydrogel. In all the examples, we treated an initial volume of water (V_{sol}) of 100 mL with a mass of the dry hydrogel (m_{dry}) of 300 mg. As expected, the maximum amount of recovered gold and the adoption kinetics strongly depends on the initial salt concentration.

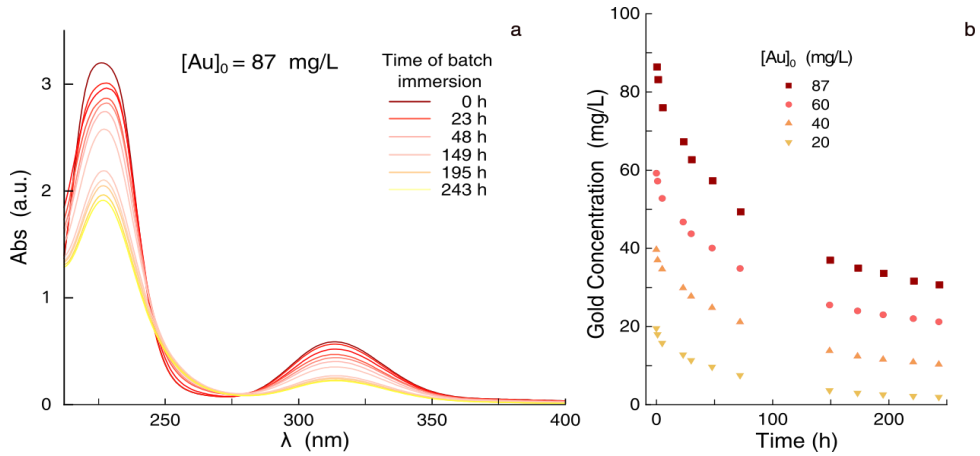

Figure 4. Stationary UV-VIS spectroscopy measures to monitor the gold absorption kinetic of the PAA1.6 hydrogel. (a) Example of absorbance measurements performed, each curve referring to an aliquot of treated pure gold solution at different times of PAA1.6 hydrogel immersion; (b) Decreasing of gold concentration (mg L^{-1}) as a function of time (h). Experimental conditions: pH=1, V_{sol}= 100 mL, m_{dry}= 300 mg.

To study the influence of the chemical structures on the gold recovery, we studied the performances of three different hydrogels immersed in an aqueous solution of gold with a concentration of 101 mg L^{-1} for 250 hours. **Figure 5a** *(left)* compares the gold concentrations in the aqueous solution before and after the hydrogel treatments. Although there is a slight dependence on the adsorbent composition, the PAA1.6 sample results in a higher percentage of gold adsorption (40% with respect to the 36% and 31% recovered, respectively, by PAA1 and PAA0.8). Moreover, as shown in **Figure 5a** *(right)*, PAA1.6 demonstrates a quicker absorption kinetic. These results are also confirmed by additional absorption kinetics data reported in **Figure 5b** for solutions with a lower initial gold concentration (20 mg L^{-1}). In this case, the maximum percentage of adsorbed gold was about 66% from PAA1.6, while the other compositions adsorbed 52-53% of the initial metal content. These characterizations showed how the composition should play a role in the gold recovery with the better performance obtained by PAA1.6, particularly for low concentration solutions. Accordingly, this material was selected for further and more detailed adsorption kinetics studies reported in **Figure 5c-d**.

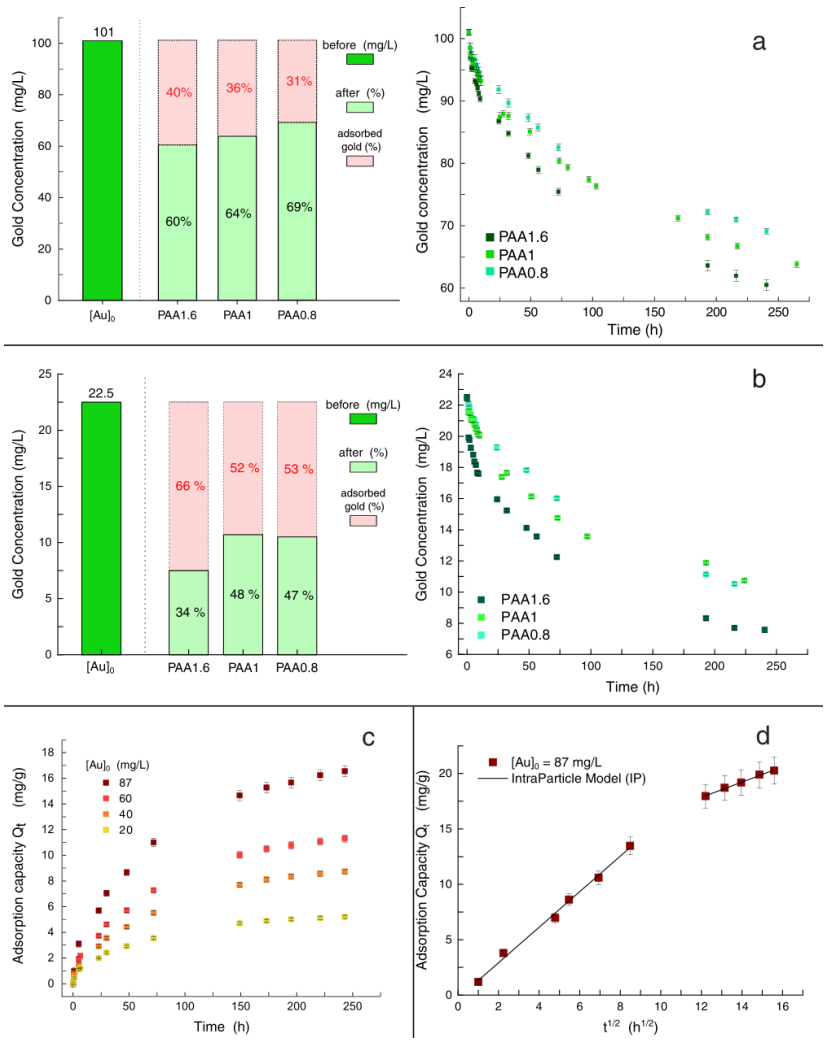

Figure 5. Comparison on hydrogel gold removing performance Gold concentration in the solution before and after the hydrogels treatment and gold concentration decay in the gold solution treated with different AAm/AAc ratio hydrogels. Experimental conditions: pH=1, V_{sol} = 100 mL, m_{dry} = 300 mg; C_0 = 100 mg L^{-1} (a) and C_0 = 20 mg L^{-1} (b). Adsorption capacity Qt presented as a function of the PAA1.6 hydrogel immersion time at various starting concentrations of gold between the lowest and the highest initial gold concentration preliminary tested (in (a) and (b)) (c). The adsorption kinetics model fitting (intraparticle model) relative to the highest starting concentration. (d)

Figure 5c reports the trend as a function of time for the *material adsorption capacity* (Q_t / mg g^{-1}), one of the most widely used parameters for characterizing and defining the adsorption performance for metals and dyes from aqueous solutions. Q_t was calculated as follows [42-48]:

$$Q_t = (C_0 - C_t) \cdot V / m \qquad (1)$$

where C_0 (mg L^{-1}) and C_t (mg L^{-1}) are the gold concentrations at time t_0 (before the hydrogel treatment) and t, respectively, V (L) is the volume of metal ion solution and m (g) is the weight of dry hydrogel.

As a straightforward consequence, the adsorption capacity at equilibrium (Q_e) is calculated considering the equilibrium gold concentration C_e as $C_{t=250h}$.
It is worth noting how the value of adsorption capacity at equilibrium (Q_e) increases with initial concentration of gold. Q_e values determined for PAA1.6 hydrogel by our analysis are 6.4, 10.6, 13.8 and 20.3 mg g^{-1}, respectively for solutions with starting salt concentration of 20, 40, 60, 87 mg L^{-1}. The higher Q_e, with a value Q_e = 124 mg g^{-1}, has been found increasing the initial salt concentration to 800 mg L^{-1} gold solution as reported in **Figure 6**. This trend, recently observed also for other systems [62], is still opposite to the one of the collected gold percentage (with recovery percentage that increased at low concentration) making the Poly(AAm-co-AAc) hydrogel particularly suitable for industrial waste solution treatment, where metals are typically present in traces.

Kinetic models

The adsorption kinetics occurring in these systems is typically complex, as it involves a series of dynamic steps that correspond to different mass transport

phenomena during adsorption. According to a simplified yet effective framework, three primary dynamic steps can be identified in the process of adsorption in porous materials [63].

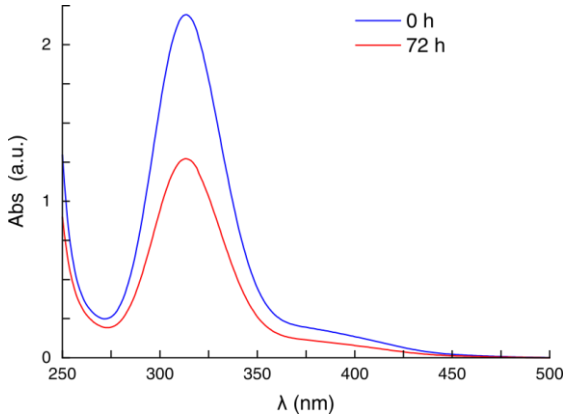

Figure 6. Determination of maximum adsorption capacity at high gold concentration. Absorption spectra of the $HAuCl_4$ solution before and after 72 h of PAA1.6 hydrogel treatment. The decrease of absorption peak corresponds to the maximum adsorption capacity Q_e = 124 mg g^{-1}. Experimental conditions: C_0 = 800 mg L^{-1}, pH=1, V_{sol} = 100 mL, m_{dry} = 300 mg.

The first step involves the external diffusion of gold ions through the aqueous film surrounding the hydrogel, driven by the concentration gradient between the bulk solution and the adsorbent surface. The second step involves the internal diffusion of ions within the hydrogel's pores, followed by the final step where ion adsorption occurs at the active sites of the adsorbent.

Among the various models, intraparticle diffusion (IP) models have proven particularly effective in describing the adsorption kinetics of metal ions and other pollutants in porous materials [64]. In this model, the kinetics is dominated by

internal diffusion of ions, i.e. the second step previously introduced.

Among the IP models, the Weber and Morris model stands out as one of the most appropriate for characterizing adsorption kinetics in liquid environments [64]. This model focuses on internal diffusion processes; and it describes the time evolution of adsorption capacity, Q_t, on slow time scale by the following expression:

$$Q_t = K_{intra}\, t^{1/2} + C \qquad (2)$$

Where K_{intra} is the kinetic constant of the process, and the C intercept is related to the processes taking place at the boundary layer between the hydrogel and liquid. The C constant takes into account the diffusion at the boundary described as an initially fast process that becomes time-independent on a long-time scale. From our experimental data we observed that the capacity kinetics show at least two different slopes in the linear plot of Q versus $t^{1/2}$, these slopes can be the evidence of two consecutive stages of mass transport, where $S_{I,2}$ coincides with $Q_{t=t1}$. The adsorption kinetics of **Figure 5d** and **Figure 7** have been described according to the Equations 3 [64]:

$$Q_t = K_{I,1}\, t^{1/2} + S_{I,1} \qquad 0 \leq t \leq t_1 \qquad (3)$$

$$Q_t = K_{I,2}\, t^{1/2} + S_{I,2} \qquad t_1 \leq t \leq t_2$$

When $t=t_1$, the first step of diffusion is completed, and adsorbates within the pores are assumed to be transferred to the active sites. Subsequently, other adsorbates from the solution can move into the pores, so migration of adsorbates from the liquid phase to the adsorbent internal surface occurs and the hydrogel exhibits a new adsorption kinetic for $t>t_1$. This two-step process, according to our interpretation, describes two internal diffusion phases characterized by

decreasing rates, as shown in **Table 3**, which contains all the model parameters derived from fitting the experimental data to Equation 3. A similar behaviour has been previously observed in other systems, where the double linear trend has been ascribed to the presence of multiple pore-size regimes [64]. The presence of multiple pore sizes is clearly evidenced by the SEM images in **Figure 10**. According to the Morris and Weber model, the intercept of the first stage, $S_{I,1}$, obtained by fitting the data, should have a negative value, and this is due to the mass transfer resistance (usually assumed as the resistance in the liquid boundary layer around the adsorbent to be tunnelled by the adsorbate) [64]. On the other hand, as reported by literature [65,66], where the constant $S_{I,1}$ value results positive, the intercept is associated with the boundary layer effect, which can be considered as the first step of the entire kinetic adsorption process. The values $S_{I,1}$ reported in **Table 3** are quite small but not zero for all tested initial gold concentrations, the positivity of the intercepts leading us to consider the boundary layer effect less relevant than the intraparticle diffusion process, which in turn leads to adsorption onto active sites present on the polymer network. This seems to suggest that some amount of the adsorbate is adsorbed by the hydrogel at the starting time of the measurement (the first gold concentration measurement in the solution is conducted 1 hour after the hydrogel's immersion due to the limited sensitivity of UV-VIS absorbance to detect small changes in adsorbed quantities over shorter time periods), suggesting that the positive intercept may simply reflect the limitations in the time resolution of the measurements. The values of $K_{I,1}$ and $K_{I,2}$ ranging from 0.2-1.6 (mg g^{-1} $h^{-1/2}$) are in the same scale of intraparticle diffusion constants evaluated for metal ions at similar concentrations [66, 67].

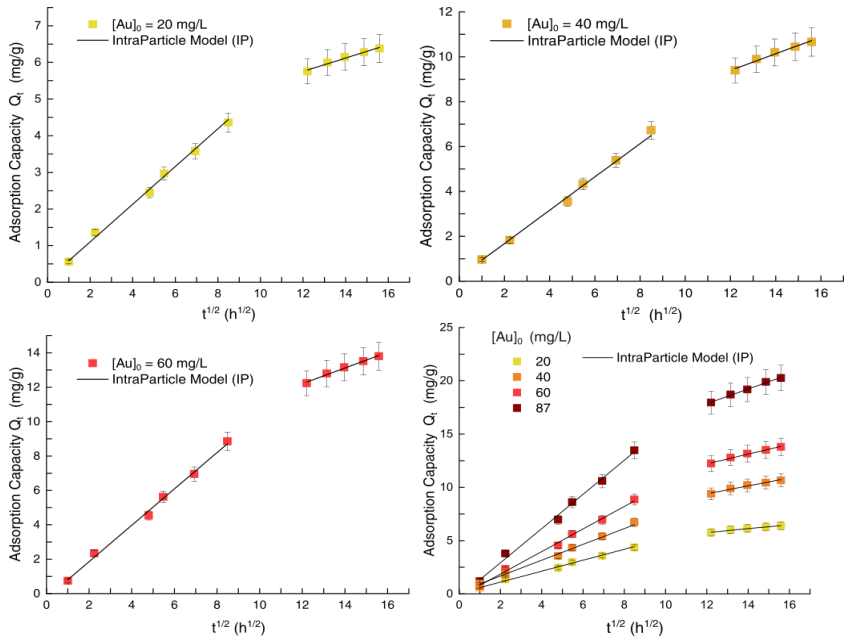

Figure 7. The Intraparticle adsorption kinetics model fitting relative to solutions with different starting gold concentrations treated with PAA1.6.

Table 3. Fitted kinetic parameter values of different stages for IP model with the associated coefficient of determination (R_i^2)[a]. Experimental Conditions: pH=1, V_{sol}=100 mL, PAA1.6 dry weight = 300 mg, room temperature (i.e. 25 °C).

C_0 (mgL^{-1})	$K_{I,1}$ ($mg\ g^{-1}\ h^{-1/2}$)	$S_{I,1}$ ($mg\ g^{-1}$)	R_1^2	$K_{I,2}$ ($mg\ g^{-1}\ h^{-1/2}$)	$S_{I,2}$ ($mg\ g^{-1}$)	R_2^2
20	0.51 ± 0.02	0.07 ± 0.05	0.994	0.182 ± 0.015	3.6 ± 0.2	0.982
40	0.74 ± 0.02	0.2 ± 0.06	0.997	0.37 ± 0.03	5.0 ± 0.4	0.976
60	1.06 ± 0.04	-0.2 ± 0.1	0.994	0.46 ± 0.02	6.7 ± 0.3	0.991

87	1.60 ± 0.08	-0.3 ± 0.2	0.991	0.69 ± 0.02	9.6 ± 0.3	0.996

[a] Coefficients of the fitting processes, is a quantity computed as $R^2 = 1 - RSS/TSS$, RSS being the "residual sum of squares" and TSS the "total sum of squares". The closer the data points are to the fitted curve, the smaller the *RSS*. R^2 varies between 0 and 1, a R^2 value close to 1 indicates a good fitting model.

Returning to the wide range of adsorption kinetic models, together with the intraparticle diffusion (IP) model that we introduced in the previous paragraphs, other approaches are frequently employed in the literature to describe the adsorption process. In particular, the pseudo-first order (PFO) model, and the pseudo-second order (PSO) model. The pseudo-first-order model, proposed by Lagergren [68], assumes that the adsorption rate is proportional to the difference between the amount of adsorbate available and the amount actually adsorbed. It is particularly effective in describing systems where diffusion mechanisms predominate, whether in the initial stage of external diffusion or the subsequent stage of internal diffusion. The PFO model has been successfully applied to the adsorption of dyes and heavy metals onto porous materials, where these diffusion processes are central to the adsorption kinetics.

In contrast, the pseudo-second order (PSO) model, developed by Ho and McKay (1996) [69], is based on the assumption that the adsorption rate is proportional to the square of the difference between the amount adsorbed at time t and the maximum adsorption capacity. This model is particularly suited for systems where the rate-limiting step involves chemical interactions at active binding sites on the adsorbent surface. As a result, the PSO model has demonstrated superior fitting accuracy in adsorption processes involving bioadsorbents or

functionalized materials, where chemical bonding at active sites plays a dominant role.

These two models can be viewed as complementary components of a unified kinetic framework. Both the PFO and PSO models are conceptually derived from the more general Langmuir kinetic model, whose physical interpretations have been extensively analyzed. It has been shown that the Langmuir kinetic model can simplify into either the PFO or PSO model, depending on boundary conditions such as the initial adsorbate concentration (C_0) and the availability of active sites on the adsorbent—whether the adsorbent is rich or poor in active sites [70]. For further clarity, Wang et al. [20] provides a detailed summary of the validity conditions for applying the PFO and PSO models.

The differential forms of the PFO and PSO models are described by the following equations, respectively:

$$\frac{dQ_t}{dt} = k_1 (Q_e - Q_t) \qquad (4)$$

$$\frac{dQ_t}{dt} = k_2 (Q_e - Q_t)^2 \qquad (5)$$

Integrating Eq. (4) and Eq. (5) for the condition of $Q_0 = 0$ yields, respectively:

$$Q_t = Q_e \left(1 - e^{-k_1(t-t_0)}\right) \qquad (4.a)$$

$$Q_t = \frac{Q_e\, t}{\frac{1}{Q_e k_2} + t} \qquad (5.a)$$

were k_1 (h^{-1}) and k_2 (g mg^{-1} h^{-1}) are the rate constants of the models and Q_e (mg g^{-1}) is the equilibrium adsorption capacity. The integrated forms of the PFO and PSO kinetic models will now be applied to analyze our experimental data.

Initially treated with the intraparticle diffusion model, which effectively represented the adsorption kinetics, this analysis aims to compare the applicability and performance of these other models in describing the system. In the **Figure 8** and **9**, the fitting plots of non-linear PFO and PSO kinetic models (Eq. (4a) and Eq. (5a)) are shown; all the fitting parameters are instead listed in **Table 4** and **Table 5**. If the reported statistical parameters R^2 are considered, it can be noted that the Intraparticle IP model, earlier presented, is the best fitting model in accordance with the experimental data.

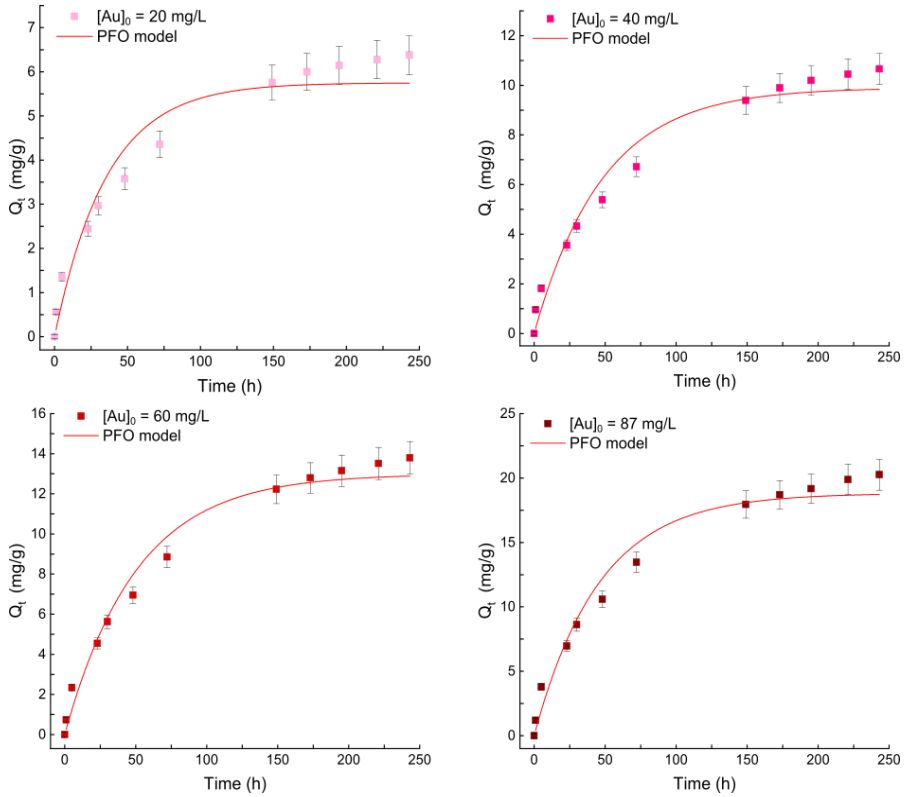

Figure 8. The Non-Linear Pseudo First Order adsorption kinetics model fitting relative to solutions with different starting gold concentrations treated with PAA1.6.

Table 4. Pseudo First Order (**PFO**) fitting parameters.

C_0 (mg L^{-1})	Q_{e_exp} (mg g^{-1})	Q_{e_fit} (mg g^{-1})	R^2
20	6.4 ± 0.4	5.8 ± 0.7	0.899
40	10.7 ± 0.6	9.9 ± 1.2	0.898
60	13.8 ± 0.8	13.0 ± 1.2	0.949
87	20.3 ± 1.2	18.8 ± 1.8	0.942

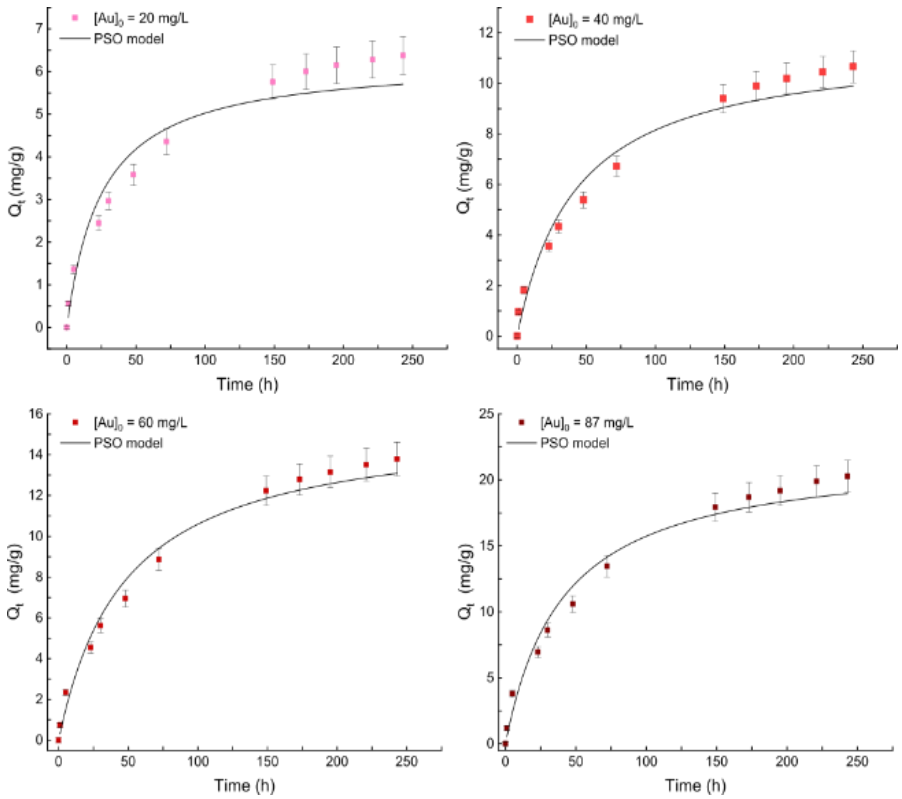

Figure 9. The Non-Linear Pseudo Second Order adsorption kinetics model fitting relative to solutions with different starting gold concentrations treated with PAA1.6.

Table 5. Pseudo Second Order (**PSO**) fitting parameters.

C_0 (mg L^{-1})	Q_{e_exp} (mg g^{-1})	Q_{e_fit} (mg g^{-1})	R^2
20	6.4 ± 0.4	6.3 ± 0.7	0.950
40	10.7 ± 0.6	11.6 ± 1.6	0.938
60	13.8 ± 0.8	15.6 ± 1.6	0.969
87	20.3 ± 1.2	22.2 ± 2.3	0.966

In some cases, such as in this one concerning Poly(Acrylamide-Acrylic Acid) hydrogels, neither of PFO and PSO models fits correctly., This suggest that the dynamic processes involve more complex mechanisms, such as diffusion within the adsorbent or multi-stage processes that cannot be fully described by those simple models. In such cases, additional factors, like diffusion limitations or surface heterogeneity, may also need to be considered to better understand the kinetics of the system For example, in Largitte and Pasquier work [71] the authors states that PFO model holds in case of non-reversible equation modelled by S+M→MS under the assumption that sorption only occurs on localized sites and involves no interaction between the adsorbed ions. This is probably not verified in hydrogels case, because of the reduction and consequent enucleation of gold nanoparticles and microflakes attached to the polymeric matrix.

Sample imaging

In addition to measuring the adsorption capacity, which is characterized by the concentration of gold ions remaining in the solution, we also investigated a series of other experimental observables related to the processes occurring within the hydrogel. These observations proved to be highly informative, enabling a more comprehensive understanding of the entire adsorption mechanism. We observed that the gold ions are not only removed from the solution but also are reduced to form elemental gold nanoparticles and microcrystalline flakes within the pores of the hydrogel. The presence of these nano- and micro-structures of metallic gold is evidenced by the reddish coloration of the hydrogel, which is attributable to plasmonic surface resonance absorption (refer **to Figure 10a**) [51]. This phenomenon can be further confirmed through direct observations using optical microscopy and Scanning Electron Microscope (SEM) imaging (see **Figures 10b-g)**. In **Figure 10a**, we present images of the PAA1.6 hydrogel taken at different time intervals, illustrating the diffusion of gold nanoparticles throughout the adsorption process. The picture shows a progressive reddish colour that appears inside the polymeric bulk material, for both the low (20 mg L^{-1}, left) and high (87 mg L^{-1}, right) gold concentration solutions. This coloured region appeared first on the external part and then propagated throughout the whole hydrogel volume. Scanning Electron Microscope (SEM) analysis on the freeze-dried samples (without any other treatment), - reported in **Figure 10b-e** - enables to observe the inner structure of the materials before the adsorption which nicely present the typical microporous morphology of polyacrylamide hydrogels or similar [55] (**Figure 10b**). After the adsorption test, homogeneously distributed nanoparticles appeared on the surfaces of the polymeric networks. In case of low gold concentration (C_0=20 mg L^{-1}), the hydrogel structure was nicely preserved also after the adsorption

and gold reduction (**Figure 10c**) while for concentration higher than C_0=60 mg L^{-1}, the interaction with gold was able to modify the 3D hydrogel structure resulting in a reduction of pore dimensions and partial closure of the pores **(Figure 10d)**. This behaviour also suggests that gold is partially present in ionic form, coordinating with several functional groups located in the pore walls. Different samples are reported in **Figure 11**; in all cases we observed the same behaviour. Regarding the nanoparticle size, in **Figure 10e** and **Figure 12**, we reported high magnification SEM that show a high dispersion of the nanoparticle dimensions in the range from 50 up to hundreds of nm or more. Indeed, for samples treated in high gold concentration, formation of microplates was also observed as shown in **Figure 10f-g**. The first is a polarized optical image where triangular and hexagonal structures can be detected with different sizes and showing birefringence, thus suggesting the formation of gold microcrystals. (Further detailed images in **Figure 11 and 12**)

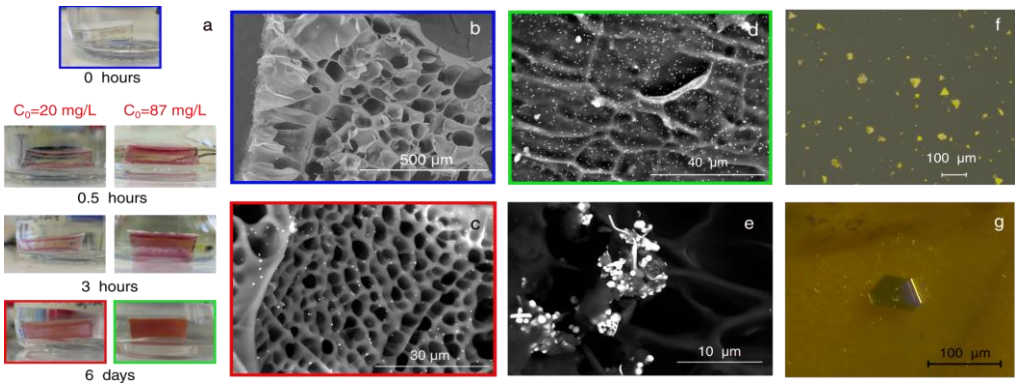

Figure 10. Formation of micrometric flakes and gold nanoparticles on the hydrogels. a) Picture of PAA1.6 hydrogels during immersion in different gold concentrated solutions as a function of time; b-e) SEM images of freeze-dried hydrogels before (b) and after immersion in a solution with initial gold concentration of 20 mgL^{-1} (c) or 87 mg L^{-1} (d, e); f-g) Optical microscopy images of an hydrated hydrogel after gold adsorption.

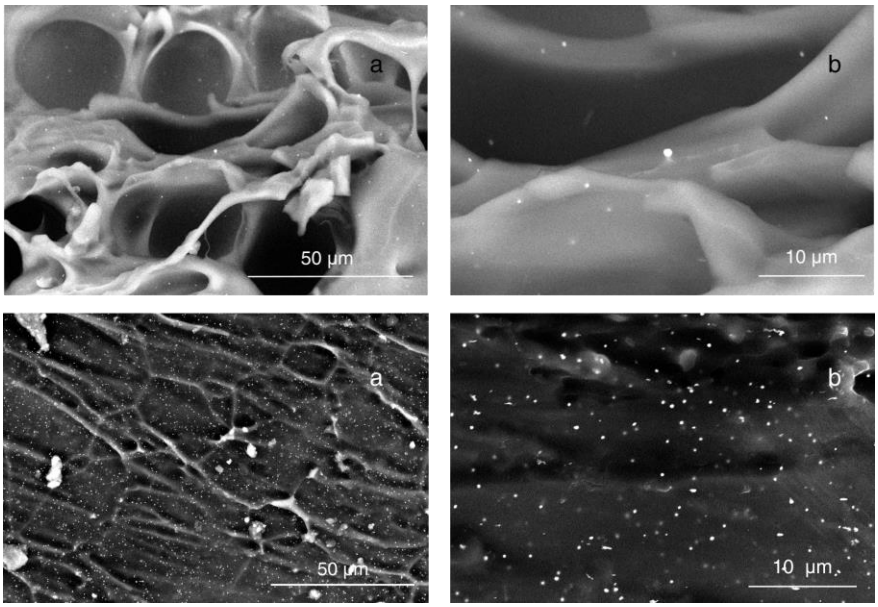

Figure 11. Example of SEM images of gold loaded PAA1.6 matrix in the lowest gold concentrated solution (C_0 = 20 mg L^{-1}) (*top*) and highest gold concentrated solution (C_0 = 60 mg L^{-1}) (*bottom*). Two different magnifications are reported: Scale bar: 50 µm (a) Scale bar: 10 µm (b).

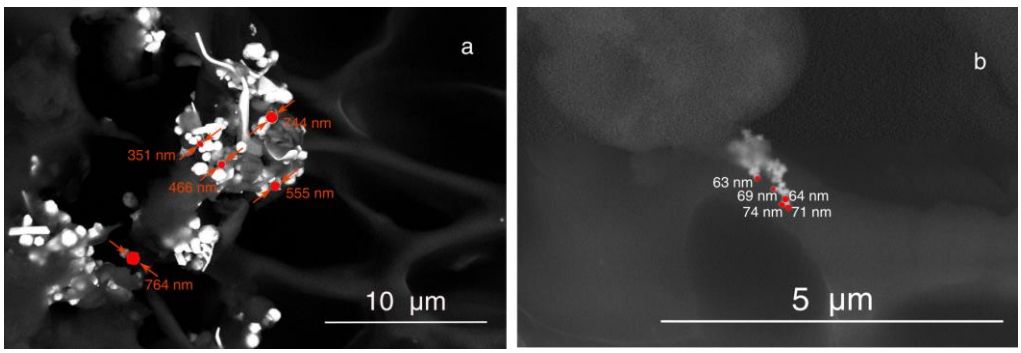

Figure 12. Estimation of gold nanoparticle sizes from SEM images relative to PAA1.6 immersed into pure gold salt solution (C_0 = 60 mg L^{-1}).

Another important observation should be done in relation to the monomer composition. Indeed, the nanoparticles formation has been observed on all the three matrices, to highlight how the application of Poly(AAm-co-AAc) hydrogels avoided the use of any additional reducing agents for the recovery of gold in elemental form. Very interestingly, despite literature examples that need heating to form the nanoparticle on polyacrylamide or polyacrylic acid, [50-53] our copolymerization approach allows the gold reduction spontaneously on the polymeric architecture at room temperature. The presence of acrylic acid seems to be critical for the process, as shown also in **Figure 13**, where a hydrogel composed only by AAm monomer is compared with PAA1.6. After immersion in a gold solution, the formation of nanoparticles at room temperature was observed mainly in the second hydrogel (the one containing acrylic acid). On the other hand, the presence of acrylamide offers several benefits, including maintaining a high equilibrium water content at acidic pH (which improves diffusion and overall adsorption performance) and simplifying material preparation, as a high gel fraction can be achieved without the need for heating, which is otherwise required to polymerize acrylic acid.

Figure 13. Optical images of PAA2 (on the left for all photos) and PAA1.6 (on the right for all photos) hydrogels after immersion in a solution containing gold. PAA2 does not contain acrylic acid as co-monomer. Experimental condition: 1 week of immersion into a solution with C_0 = 100 mg L^{-1}, pH=1.

2.2.3. An example of application: gold adsorption in a mixed metal industrial wastewater

The final step of this work is the use of the selected Poly(AAm-co-AAc) hydrogel matrix (PAA1.6) as adsorbent in a mixed noble metal ion solution which closely mimics the realistic condition of an industrial wastewater, chosen on the basis of Cabro S.p.A. water residue. The target solution includes different precious metal ions (Au(III), Pd(II), Pt(IV), Ru(III), Rh(III) and Ir(III)) at quantities not exceeding 20 mg L^{-1} for each metal, and determines the working conditions in an acid environment (pH=1). The major challenges for the treatment of this type of solution is the selective recovery of one metal with respect to the others, together with a low metal concentration that reduces the number of available treatment techniques. Indeed, recent works on hydrogel absorbent demonstrated a high quantity of recovered gold but without selectivity when the metals of platinum group are present [20]. In this regard, our hydrogel may offer an advantage in selectivity if the primary mechanism for gold recovery is nanoparticle reduction, rather than complexation or electrostatic interactions between the ions and the functional groups of the adsorbent. Under these conditions, selectivity is achieved if the proposed material selectively reduces gold ions without affecting other metal cations. The already demonstrated gold adsorption has been obtained at a pH around 1 allowing, at least in principle, to eliminate the adsorption of the other metal ions due to high matrix effect interaction (e.g. acrylic acid is protonated disfavouring interaction with cations) [72]. The treatment of the mixed metal solution followed a batch test, where the hydrogel is directly immersed in the solution for different times (**Figure 14a**). After one week, the initial orange solution became almost colourless, while the hydrogel changed colour (see **Figure 15**). A detailed quantification of the metal concentration after the hydrogel adsorption is reported in **Figure 14b**, while the

relative recovery percentages are shown in **Figure 14c**. In this case, the concentration of each metal has been determined by ICP-OES (Inductively coupled plasma - optical emission spectrometry) elemental analysis since the application of UV-visible spectroscopy was not possible for this complex solution.

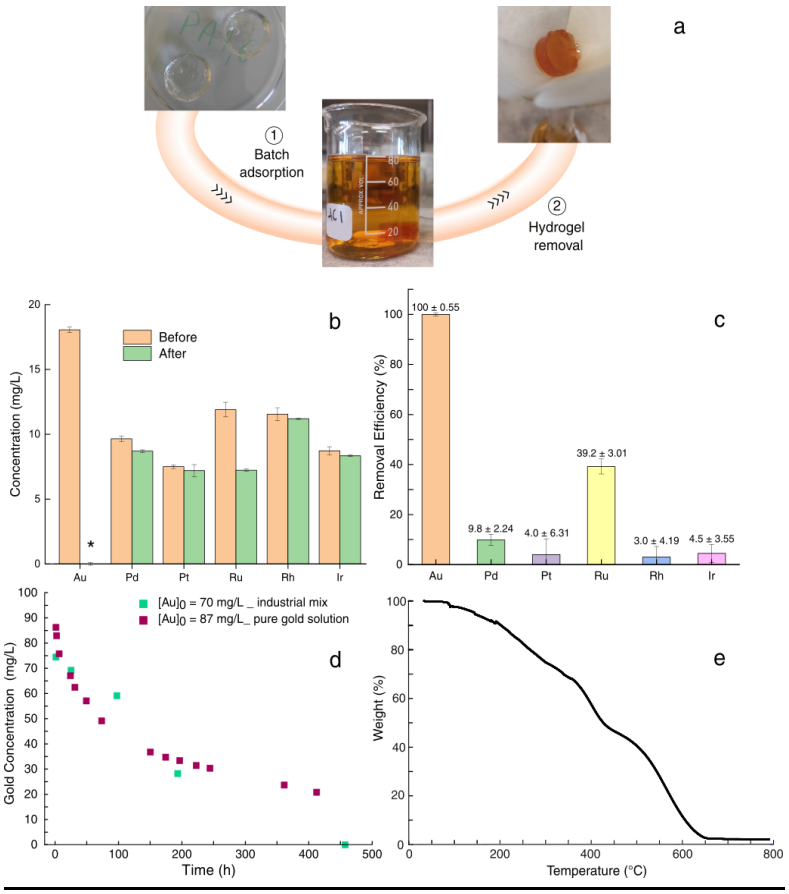

Figure 14. Treatment of mixed metal solutions with Poly(AAm-co-AAc) hydrogels. a) Steps for gold selective separation from a solution mimicking industrial waste. b) Concentration of different metals in a mixed solution before and after the PAA1.6 hydrogel treatment. Measures are performed by means of ICP-OES elemental analysis. c) Percentage of metal ions recovery for PAA1.6 immersed (1 week) into the mixed metal solution. d) Comparison of PAA1.6 hydrogel adsorption performances between a

pure gold solution (red squares) measured by UV-Vis spectroscopy and a mixed metal solution (turquoise squares) measured by ICP-OES. e) Thermogravimetric analysis of PAA1.6 hydrogel matrix.

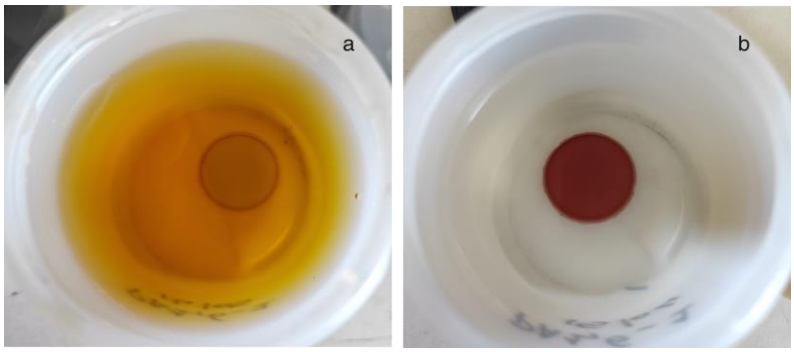

Figure 15. Mixed metal ions solution appearance before and after PAA1.6 hydrogel treatment. Pictures of the solution after 1h (a) and 1 week (b) of hydrogel immersion.

After one week immersion, PAA1.6 was able to adsorb almost completely the gold present in the solution (recovery of 18 mg L^{-1}) with the formation of micro and nanoparticles also in this case (see **Figure 16** for SEM images). As supposed initially the recovery occurs with high selectivity with respect to the competing cation. Indeed, cations like Pt(IV), Rh(III) and Ir(III) were not adsorbed on PAA1.6 while Pd(II), Ru(III) were adsorbed only in low amounts (0.8 and 5.7 mg L^{-1} respectively, which correspond to 9.8% and 39% of recovery). After 4 days of treatment, the extraction selectivity of Au(III) over other adsorbed metal can be calculated as 55.07 times more selective over *Pd(III)* and 35.56 times over *Ru(III)*.

The same analysis conducted at different immersion time is reported in **Figure 17a**. Indeed, after 24 h the gold recovery was about 36.5%, and after 72 h the percentage was increased at 98.3%. During this time, also the ruthenium was gradually adsorbed (recovery 22% and 40.9% at 24 h and 72 h) demonstrating

how the adsorption processes of the two metals are simultaneously. Thus, diminishing the immersion time of the hydrogel did not significantly improve the selectivity. Regarding the adsorption kinetics, **Figure 14d** shows the comparison between the hydrogel adsorption performance in a pure gold solution and in a mixed metal one containing gold with a similar concentration. The adsorption trends are quite similar, despite these measurements being performed using different techniques, UV-Vis spectroscopy and ICP-OES, confirming the promising performance of Poly(AAm-co-AAc) hydrogel material in gold acid solutions with or without competitive precious metal ions. A difference was observed in the residual gold concentration; in the mixed solution, the hydrogel achieved complete recovery (within the detection limits of the ICP-OES analysis used), suggesting the potential for recovery even at lower concentrations. A final consideration regarding the potential use of Poly(AAm-co-AAc) hydrogel pertains to the ultimate gold recovery from the material. This process could be carried out either by dissolving the formed nanoparticles or by thermally degrading the matrices to recover the solid metals. Regarding the former, an example of gold elution by aqua regia immersion is shown **in Figure 18** but this approach again results in an acidic solution with high metal dilution. For the latter, it is important to choose the matrix appropriately since it must lead to a low amount of solid carbon residue (ideally zero residue) after combustion. An insight of this aspect, it is shown by the thermogravimetric analysis (TGA) reported for PAA1.6 in **Figure 14e**. The hydrogel has already lost 50% of its original (dry) weight at 400 °C and no solid residue is observed at 600 °C. A comparison with a commercial resin used for metal recovery is presented in **Figure 19**. The TGA analysis revealed a potential issue with the combustion of commercial materials (i.e. MTC1500 industrial resin), which is related to their formulation. On one hand, composite formulations can enhance adsorption capacity (albeit without metal selectivity);

on the other hand, the high solid residue remaining after thermal treatment poses a significant challenge, hindering the recovery of solid metals with high purity.

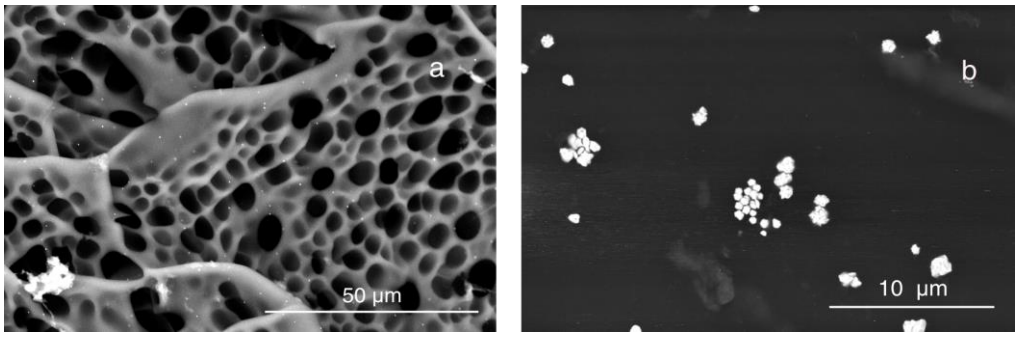

Figure 16. SEM images of PAA1.6 hydrogel after the immersion in a mixed metal ion solution provided by industry. The gold initial concentration C_0 was around 10 mg L^{-1}.

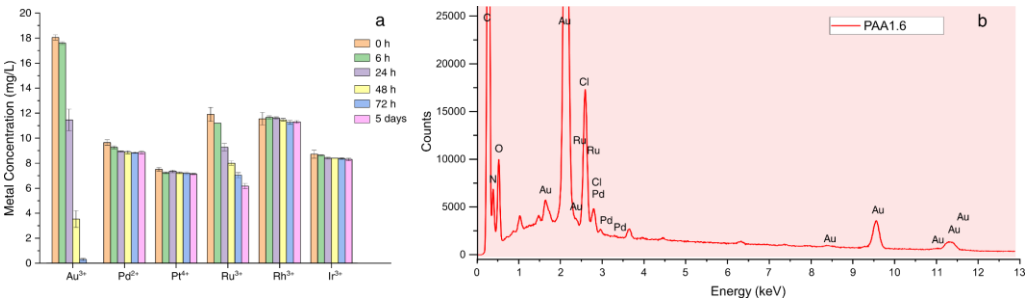

Figure 17. More insight on gold recovery in a mixed metal solution. Concentration of residual metal ions (mg L^{-1}) in the mixed solution as a function of PAA1.6 hydrogel immersion time. Measurements performed by ICP-OES elemental analysis thanks to Cabro S.p.A. (a) EDS measurements of PAA1.6 hydrogel after immersion (1 week) in a mixed solution containing Au, Pd, Pt, Ru, Rh, Ir furnished by Cabro S.p.A. industry. (b)

Figure 17b reports the EDS measurement performed on PAA1.6 hydrogel after the immersion in a mixed metal solution. It's possible to recognize the gold characteristic peaks, some peaks relative to ruthenium and just down to traces of

palladium; consistent with the measurements of selectivity (**Figure 14b** and **17a**).

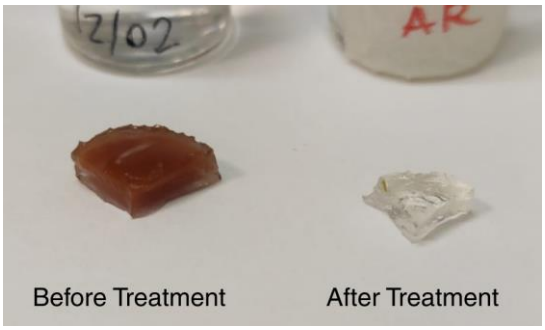

Figure 18. Gold elution from the hydrogel. Picture of a gold loaded PAA1.6 material before and after the immersion into aqua regia (1 day).

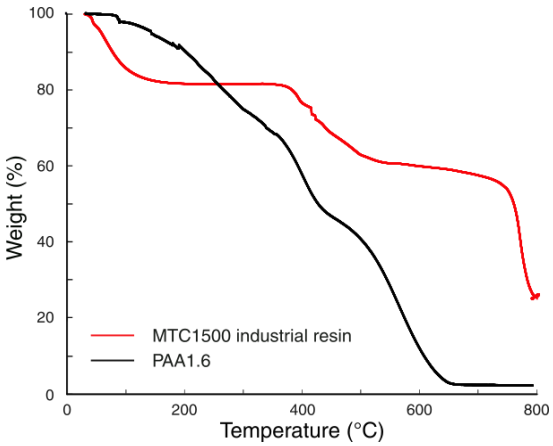

Figure 19. Comparison of TGA measurements between PAA1.6 hydrogel and MTC1500 industrial resin. The latter is a macroporous polystyrene cross-linked with divinylbenzene, furnished by CABRO S.p.A.

Towards potential industrial scalability, preliminary cost evaluation highlights the promising economic viability of our system. The total cost of producing the hydrogel required to recover 1 g of gold is below 0.1 € (based on the maximum Q_e reported in this study, see **Table 6**). Notably, the whole recovery process is

energy efficient, as no heating or cooling is necessary for both the polymerization of PAA1.6 and the adsorption process. Additionally, the wastewater can be conducted without the need for further chemical treatment (e.g. pH adjustment). This aspect represents a clear advantage when comparing our hydrogel-based adsorbents with the conventional methods like activated carbon and ion exchange resins. Our hydrogels offer an effective and low-cost approach for the removal of heavy and precious metals, with further optimization – such as by modulating the functional groups to expand the range of adsorbed species – our system has the potential for long-term use through recycling after gold elution, making it a highly competitive alternative for industrial applications.

Table 6 . Evaluation of the materials cost

Substance	*Cost (€) **	*Quantity*
Acrylamide	33.00	1 Kg
Acrylic Acid	47.30	1 L
N,N'-Methylenebisacrylamide	47.90	100 g
Ammonium Persulfate	48.50	0.5 Kg
N, N' Dimethylethylenediamine	30.00	0.250 L
PAA1.6 hydrogel	**9.13**	**1 Kg**
Gold	**78.26 ****	**1 g**

* prices are taken from Merck quotation at January 2023 (except for gold)
****** taken from the website Cabro S.p.A. industry in October 2024

2.3. CONCLUSIONS

In summary, we demonstrated how hydrogels prepared by copolymerization of acrylamide and acrylic acid (and without any further additives) can be used as efficient adsorbents for gold ions in acid solutions. The materials demonstrated the ability to reduce this metal, forming particles of various sizes, ranging from 50 nm nanoparticles to microplates several hundred microns in size, all of which were homogeneously dispersed within the polymeric matrices. This process was effective even at concentrations lower than 20 mg L^{-1}. The hydrogel's inherent reduction capability eliminated the need for additional reductants, offering a significant advantage in reducing the environmental impact associated with the use of reducing agents and energy consumption. Moreover, the behaviour observed here for metal recovery could also be used for the synthesis of nanoparticle catalysts that are well-dispersed and supported within a polymeric matrix.

A remarkable feature of Poly(AAm-co-AAc) is the possibility to obtain a good separation of gold by other precious metals present in the solution and competing with the adsorption, a behaviour which is rarely reported on other hydrogels used for gold recovery. We hypothesize that selectivity is mainly driven by the recovery mechanism of the hydrogel where the selective gold reduction occurs at acid pH while other metals remain unaffected. At this pH, interactions such as electrostatic binding and complexation between the functional groups and other ions are less favoured.), Our systems allowed for a complete selectivity from cations like Pt(IV), Rh(III) or Ir(III) and a good selectivity towards Pd(II) and Ru(III). The higher limitation for specific adsorption is represented by the presence of ruthenium with a ratio of 0.31 in weight of the adsorbed metals (in the proposed example). Indeed, further studies should be conducted to efficiently remove one of the two metals by the hydrogel matrices by appropriate elution to

achieve the complete metal separation. The dissolution of metals, including elemental gold, is a key aspect for enabling the reuse of the hydrogel in multiple adsorption cycles. Although this study demonstrates gold dissolution using aqua regia, simpler and more environmentally friendly methods are necessary to enable effective adsorbent recycling. Future efforts will focus on introducing additional chemical groups to modify selectivity, potentially enabling the recovery of other precious metals, for example, under different pH conditions. As a final remark, we would like to emphasize that the present hydrogels are already suitable for gold recovery in various applications, including metal recycling from e-waste and treatment of residues from the jewellery industries.

2.4. EXPERIMENTAL SECTION

2.4.1. Materials

Acrylamide (AAm), Acrylic acid (AAc), *N,N'*-Methylenebisacrylamide (BIS), Ammonium PerSulfate (APS), *N,N,N',N'*-tetramethylethylenediamine (TEMED), tetrachloroauric(III) acid trihydrate ≥ 99.9% ($HAuCl_4 \cdot 3H_2O$), and Hydrochloric acid (HCl) were purchased from Sigma-Aldrich. All chemicals appearing in this work were utilized without any further manipulation. All other metal salts (containing Pt(IV), Rh(III), Ir(III), Pd(II), Ru(III)) have been provided by Cabro S.p.A.

2.4.2. Hydrogel synthesis

A solution of monomers (AA and AC in different ratios reported in **Table 2**) and BIS was prepared deionized water. Then a 10% m/V solution of APS was added to achieve a final concentration of 0.2% of initiator and a 10% m/V solution of

TEMED was added to achieve a final concentration of 2% The free-radical polymerization occurred in 1 hour at room temperature for PAA1.6 and at 60 °C PAA1 and PAA0.8.

2.4.3. Hydrogel characterization

The Gel Fraction (GF) indicates the percentage of the solid monomers that effectively are incorporated inside the network. It was calculated by the following equation:

$$GF\ (\%) = (Wd_2 / Wd_1\ ) \times 100 \qquad (6)$$

Where Wd_1 (g) Wd_2 (g) are the weight of the dry material just after its preparation (Wd_1) and the weight of the dried gel after immersion in water (to eliminate unpolymerized material, Wd_2).

The Equilibrium Water Content (EWC) has been determined by gravimetric methods and indicates the percentage of water retained by the gel network in its fully swollen state. It was calculated by the following equation:

$$EWC\ (\%) = (Ws - Wd\ ) / Ws \times 100 \qquad (7)$$

where Ws(g) and Wd(g) are respectively the weight of the fully swollen and the weight of completely dried hydrogel respectively. The measurements were repeated in triplicate and in two different pH conditions (neutral and strongly acid buffer solution), with the results showed in the **Figure 3**.

Polarized Optical Microscopy (AxioLab5, Zeiss) (POM) and Scanning Electron Microscopy (FlexSEM 1000, Hitachi) (SEM) images were performed to characterize the internal structure of hydrogel before and after the metal ions

adsorption. Moreover Energy-Dispersive Spectroscopy (EDS, using SEM Inspect-F microscope) measurements on hydrogel matrix have been performed in the case of mixed solutions, to confirm the presence of elemental gold on adsorbent material and check the minor contribution of other metals present. The thermogravimetric measurements have been performed using SDT Q600, T.A. Instruments thermogravimetric analyzer, furnished by Cabro S.p.A industry. The measures were carried out in a temperature range from 20 to 800 ° C, with a heating rate of 2 °C / min under an air atmosphere.

2.4.4. Metal ions adsorption measurements

The batch adsorption tests were performed by putting the poly (AAm-co-AAc) hydrogel (after swelling of 300 mg of dry materials) in 100 mL of solution with different initial gold concentrations (20, 40, 60, 87 mg L^{-1}) or mixed metal ions solution. The gold solutions were prepared by dissolving tetra-chloroauric(III) acid ($HAuCl_4$) in a previously prepared 0.2M HCl buffer. The final pH of the solution was adjusted to pH=1. The measures of residual gold concentration in pure gold solutions were performed by means of UV-Vis Spectroscopy (LAMBDA 950 UV/Vis spectrophotometer, PerkinElmer and V650 UV/Vis spectrophotometer, JASCO - Grenoble). The mixed metal cations solution has been furnished by Cabro S.p.A., making it starting from disposal of precious metal ions solutions already existing in the company. The final composition contains around 20 mg L^{-1} of each metal and has a pH=1. In this case the technique used to follow the residual metal cations concentration is the ICP-OES Spectroscopy elemental analysis (5110 ICP-OES, Agilent, measures provided by Cabro S.p.A.). The calculation of gold residual concentration was carried out using the Lambert-Beer formula, expressed as follows:

$$A = \varepsilon C l \qquad (8)$$

where A is the absorbance value, ε [$cm^{-1}mg^{-1}L$] is the molar extinction coefficient of $HAuCl_4$, C [mg L^{-1}] is the gold ions concentration and l [cm] is the path length (i.e. the cuvette thickness). In order to proceed with the adsorption experiments and follow the decay of gold concentration in the treated solution, the molar extinction coefficient ε relative to the $HAuCl_4$ characteristic absorption peak wavelength was estimated as showed in the **Figure 20**.

Extraction of selectivity of Au(III) over other adsorbed metal in the mixed solution is calculated according to the following equation:

$$\text{Selectivity of Au(III) over other metal } M^{+} = (C(M)_{final}/C(Au)_{final})/(C(M)_{initial}/C(Au)_{initial}) \quad (9)$$

Where $C(M)_{final}$ and $C(M)_{initial}$ are respectively the concentrations of the metal M before and after the adsorption process.

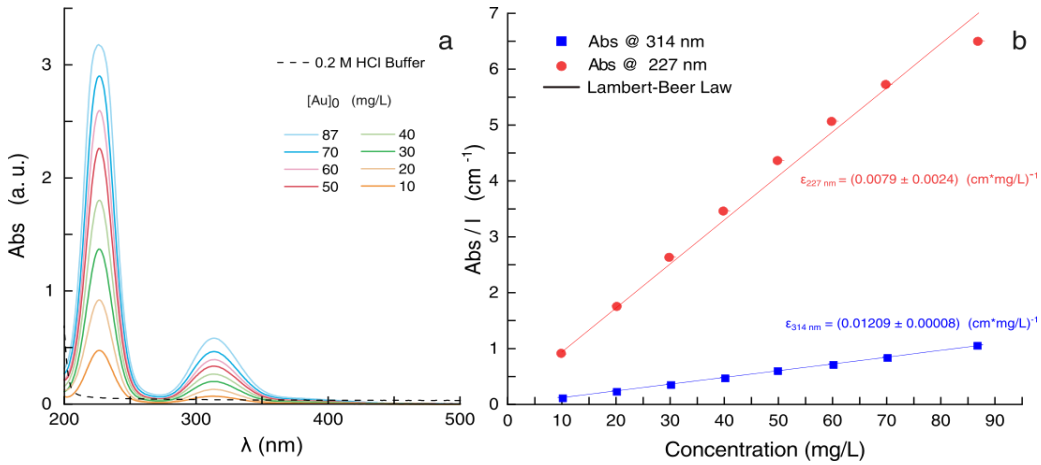

Figure 20. Determination of molar extinction coefficient of $HAuCl_4$. (a) Example of $HAuCl_4$ acidic solution (pH 1) absorption spectrum. (b) Calibration curve to determine the molar extinction coefficient. ε [L $cm^{-1}mg^{-1}$] at λ=314 nm (maximum of one characteristic absorption band for $HAuCl_4$ acidic solution) is taken as reference for quantification of gold concentration. The coefficient is estimated from the fit in the

graph (b) as $\varepsilon_{314nm} = (0.01209 \pm 0.00008)\ cm^{-1}mg^{-1}L$ in accordance with previous studies [73].

3. Cryogels: a novel porous material for recovery of gold from other noble metals

3.1. INTRODUCTION

In this chapter, we explore an alternative method for preparing adsorbents, building on the promising results discussed in the previous chapter. The objective was to modify the material's microstructure and porosity to gain deeper insight into how these parameters influence the adsorption capacity, kinetics, and selectivity, particularly for gold ions in complex mixtures with other precious metals. While hydrogels have shown good performance for selective metal recovery, we hypothesized that a more highly porous structure, such as that of a cryogel, could further enhance the gold adsorption process.

Cryogels are a class of highly sieve-like materials synthesized through cryo-polymerization at subzero temperatures, resulting in a three-dimensional network with interconnected macropores. During the process, a polymer solution is frozen and allowed to polymerize in the frozen state, creating a sponge-like structure with high permeability and a large surface area. This architecture can enhance diffusion rates and adsorption efficiency and unlike traditional hydrogels which form porous networks at room temperature, cryo-

polymerization offers an additional level of control over the material's macrostructure [74]. The macroporous nature of cryogel materials provides a significant advantage as adsorbents in batch adsorption processes and allows also continuous water flow throughout the sponge-like polymeric structure [75-77], opening up possibilities for their use in filtration columns, a feature not typically achievable with hydrogels, where continuous water flux is often slow or not possible.

The state of the art in cryogel-based adsorbents for metal remediation has demonstrated promising results in various applications, such as the removal of heavy metals and organic pollutants from contaminated water. Research has shown that the combination of high porosity, mechanical stability, and the ability to fine-tune the polymer network by incorporating different co-monomers makes cryogels particularly effective in selective adsorption. While their versatility has been widely exploited for the adsorption of various contaminants, their application in the selective recovery of precious metals, especially gold, remains underexplored [75]. The materials shown in the following sections, prepared using acrylic acid as the primary monomer, with co-monomers such as acrylamide or hydroxyethyl acrylate (HEA) exhibit a highly interconnected macroporous structure that significantly should enhance gold adsorption performance compared to standard hydrogels. The incorporation of these co-monomers allows for increased functional group density and better structural integrity, which should, in turn, lead to improved selectivity and capacity for gold recovery.

In the following sections, we will present the results of batch adsorption tests conducted with acidic solutions at room temperature as for the hydrogel of **Chapter 2**. These tests demonstrate the cryogels ability to recover gold ions efficiently while simultaneously reducing them to elemental nanoparticles,

which are uniformly distributed throughout the polymeric network. Notably, other precious metals, including Ru, Pd, and Pt, remain in the solution, highlighting the material's high selectivity for gold. The enhanced performance of the cryogel over standard hydrogels, as outlined in Chapter 2, underscores the importance of tailoring the material's microstructure and porosity to achieve the desired adsorption characteristics.

3.2. RESULTS AND DISCUSSIONS

3.2.1. Material preparation and characterization

The cryogel were prepared by cryopolymerization of an aqueous mixture containing acrylamide (AAm) or hydroxyethylacrylate (HEA) as major monomer, acrylic acid (AAc) as co-monomer, and N,N'-Methylenebisacrylamide (BIS) as crosslinker with the procedure briefly described in **Figure 21.** After addition of ammonium persulfate (APS, as an initiator) and tetramethyl-ethylenediamine (TEMED, as a co-initiator) to the other monomers, the final formulation was freezed at -18 °C to obtain the cryo-polymerization [74]. Indeed, during the freezing process, most of the solvent (e.g. water) is frozen while the dissolved monomers are concentrated in small non-frozen regions, the so called ‘‘non-frozen liquid microphase’’. The polymerization can take place in this segregated phase with the crystals of frozen solvent acting as pore-tamplate. After thawing, a polymeric system with large, interconnected pores is formed. One of the important parameters affecting the performance of porous hydrophilic materials is pore structure that can be controlled by different parameters, such as the freezing temperature, the concentration of monomers in the initial reaction mixture and the type and content of a crosslinker. In this work, the monomers concentration was fixed

(0.3 M of AAc and 1.3 M of the co-monomer) and the concentration of crosslinker was variable (97 or 149 mM). The complete list of sample compositions is provided in **Table 7**. Taking in mind that all the formulations contain the same amount of AAc, the cryogels are called Cryo-A1 and Cryo-A2 if they contain acrylamide as co-monomer (but different crosslinker amounts) or Cryo-H to indicate the presence of HEA.

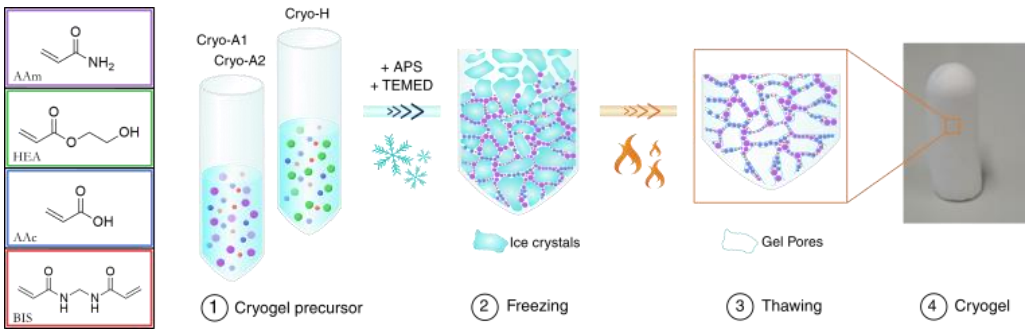

Figure 21. Cryogel Preparation. Chemical structures of monomers and scheme for the preparation route of the adsorbents (1,2,3). On the right, a picture of the final cryogel is shown (4). The materials have been prepared by different mixture of Acrylamide (AAm), Hydroxyethyl Acrylate (HEA) and Acrylic Acid (AAc) and the crosslinker *N,N'*-Methylenebisacrylamide (BIS).

Table 7. Compositions of the monomeric formulations for the cryogel adsorbents.

	AAm (M)	**HEA** (M)	**AAc** (M)	**BIS** (mM)
Cryo-A1	1.3	-	0.3	97
Cryo-A2	1.3	-	0.3	149

Cryo-H	-	1.3	0.3	97

The different mixtures of monomers and crosslinker were chosen to investigate the potential impact of molecular composition on absorption capabilities and kinetics, because of the presence and combination of different functional groups onto the polymeric network. Co-polymers of acrylamide and acrylic acid were chosen on the basis of our previous results showing how their hydrogel acted as reducing agents for gold cations in solution [24]. Since acrylic acid was demonstrated essential for the reduction process, we explored here the substitution of acrylamide with a non-toxic monomer widely used, the hydroxyethyl acrylate, which also confers different exposed functional groups. In the end, BIS concentration has been varied in one co-monomer composition since this parameter greatly affects the water penetration inside the cryogel [76,77].

After synthesis, the chemical composition of cryogel was characterized by ATR-FTIR spectroscopy measurements, reported in **Figure 22a**. According to the literature [30, 31] all spectra present a broad peak around 3350 cm^{-1}, corresponding to the stretching of O-H bonds. The distinct narrow signal that appears at 1725 cm^{-1} is ascribed to the strong vibration of C=O ester groups. This feature appears only in the Cryo-H spectrum due to the presence of HEA in the polymer. More broadly, the 1725-1600 cm^{-1} wavenumber range is related to C=O double bond, which may represent amide or acid carbonyl groups. Another characteristic IR signal of HEA, also found only in the Cryo-H sample, appears in the 1300–1000 cm^{-1} range and is associated with C–O bonds in ester or ether groups. The peak at 2930 cm^{-1} is associated to the C-H groups stretching and being common to all cryogel compositions. On the other hand, the signal that

appears at 3190 cm^{-1} corresponds to the stretching of N-H groups and is only present in the AAm containing cryogels. Moreover, **Figure 22b** shows the thermogravimetric analysis (TGA) of all the materials. The thermal degradation is strongly influenced by the chemical composition. All cryogels initially lose weight up to 100 °C due to the evaporation of residual water. When AAm is combined with AAc, the first loss is followed by a 50% reduction of its original dry weight at 400 °C, with no solid residue remaining at 600 °C. In contrast, the third composition performs significantly better; when HEA replaces AAm, an 80% weight loss is observed around 350 °C, and no solid residue remains at 500 °C. The comparison with a commercial resin used for metal recovery is presented in **Figure 23.** Compared to the hydrogel material tested in the previous chapter, the cryogel matrix exhibits a slightly faster thermal degradation process. In fact, in that case, no solid residue is observed even at 600 °C **(Figure 19).**

SEM images of the lyophilized samples are shown in **Figure 22c** confirming the typical porous and highly interconnected structure of all AAc-based cryogel compositions. More images at different magnification are also provided in **Figure 24a**, through which it is possible to estimate a pore size not exceeding 100 μm. Many SEM measurements allowed for statistical analysis of the pore sizes, resulting in a histogram distribution peaked around 20-30 μm for all the samples (see **Figure 24b**). Another main advantage of cryogels with respect to standard hydrogel can be observed in their swelling kinetics. Indeed, the maximum swelling of the cryogel can be obtained just after a few seconds of immersion of the dry materials.

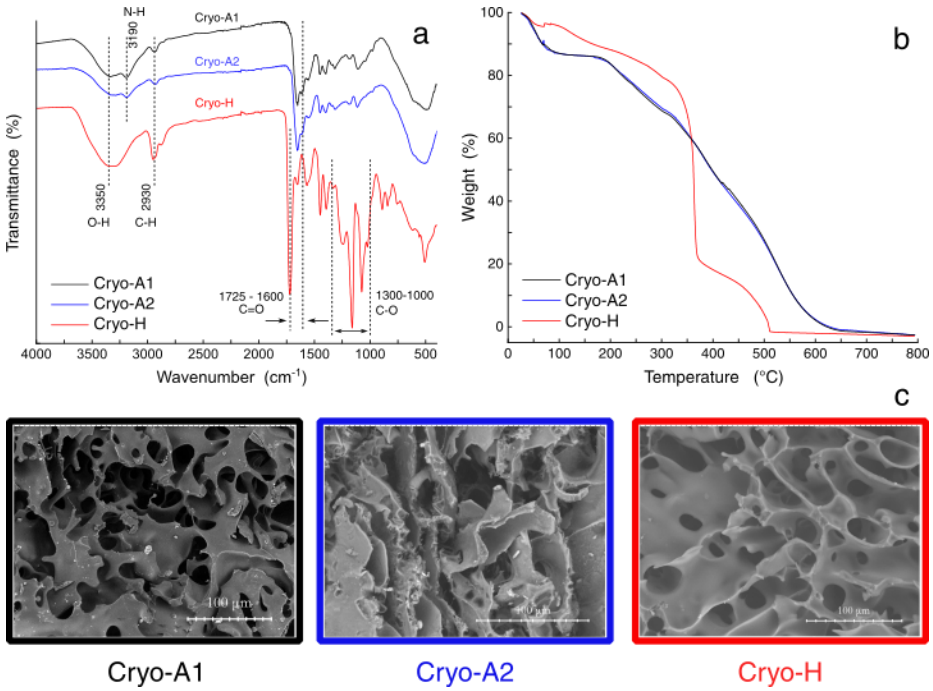

Figure 22. Material Characterization. ATR-FTIR spectra (a) and Thermogravimetric analysis (TGA) (b), both for Cryo-A1 (black), Cryo-A2 (blue) and Cryo-H (red); SEM images of the clean polymeric matrices of the cryogels; with the 100 µm scale bar. (c)

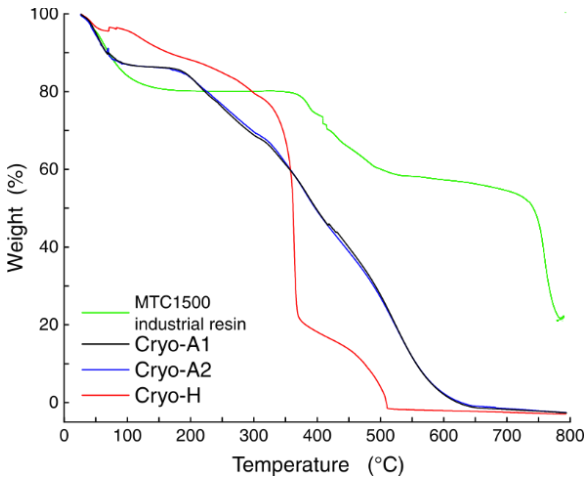

Figure 23. Comparison of TGA measurements between AAc-based cryogel and MTC1500 industrial resin. The latter is a macroporous polystyrene cross-linked with divinylbenzene, furnished by CABRO S.p.A.

Figure 25a shows the fast swelling process that occurs in a AAc-based cryogel matrix, a behaviour that is strictly related to porous structures obtained at micrometric level thanks to the cryopolymarizatio and a confirmation on the interconnected nature of the porous architecture. Other Typical parameters that characterize the adsorbents are the Equilibrium Water Content (EWC) and the water flow rate shown in **Figure 25b-c** and also reported in **Table 8**.

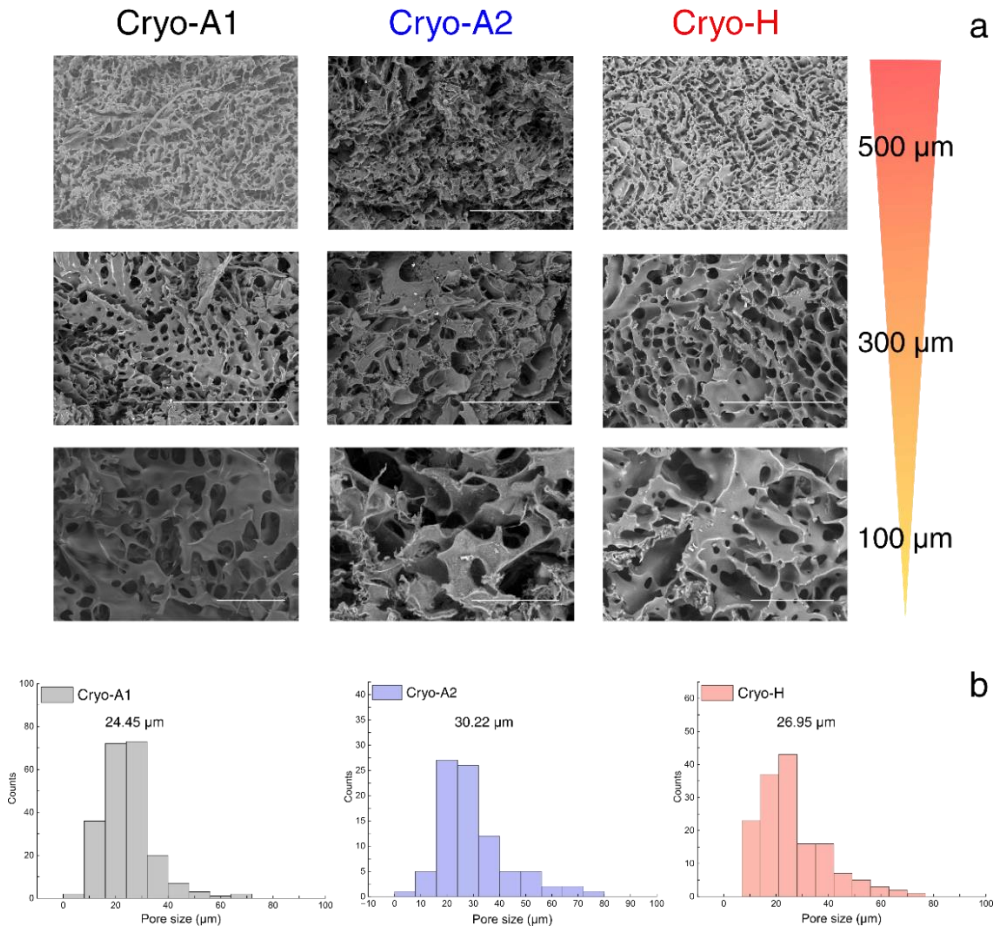

Figure 24. Additional SEM images of the cryogel. Images at different scale bars (500 µm, 300 µm and 100 µm from top to bottom, respectively) of cryogels internal structure (a). Pore size distribution estimation by a statistical analysis using SEM measurements (b).

Table 8. Equilibrium Water Content both in distilled water and 1M HCl solution and estimation of water flow rate for all cryogel compositions.

Sample	EWC in H_2O[c]	EWC in HCl 1M[c]	water flow rate (mL h^{-1})
Cryo-A1	94.5%	92.2%	5.5
Cryo-A2	93.9%	91%	277.5
Cryo-H	92.4%	88%	190

[c] values are the medium of the three repeated measurements.

The first parameter highlights the capabilities of the materials to uptake a large amount of water and it has been tested in both deionized water and a 1M HCl buffer solution. The need for this specific highly acidic pH arises from the requirements of the company, which, as will be shown later, provided a multi-metallic waste solution under these conditions. Solutions with a similar pH are frequently employed when metal cation solutions are obtained from e-waste dissolution [39], highlighting the relevance of this scenario for the recovery of precious metals. The EWC percentages demonstrate optimal performance, ranging from a minimum of 88% to a maximum of almost 95%.

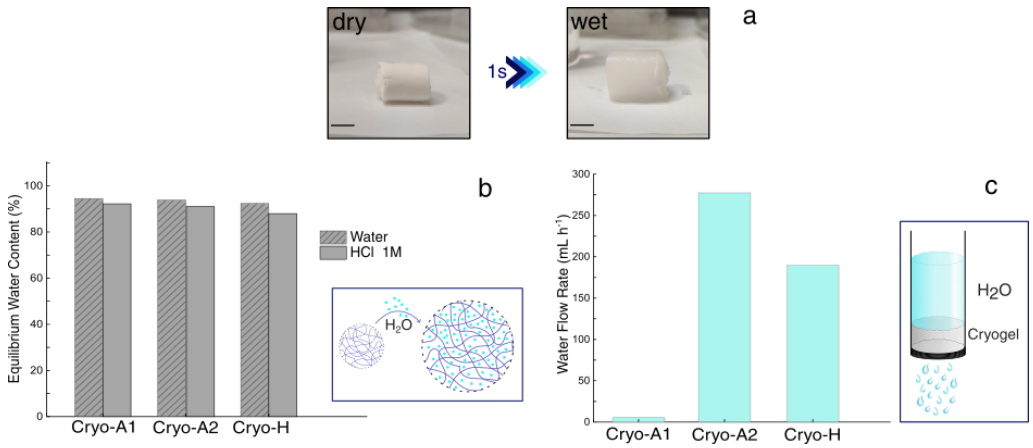

Figure 25. Swelling behavior of the cryogels. Visual appearance of a little portion of the Cryo-A1 material before and after immersion in deionized water, scale bar: 1 cm (a); Equilibrium Water Content (b) and water flow rate (c) of the different cryogels. Flow rate was measured as the amount of water passing through a 2 cm cryogel column in 1 hour at a constant hydrostatic pressure (equal to 1 m of water column).

It is important to note how the dependence on the solution pH of this parameter is greatly reduced with respect to conventional hydrogels. In fact, while a decrease of at least 16% was observed in hydrogels with the same monomeric composition [24], here the reduction in water content due to the pH change reaches a maximum of only 4%. Moreover, the macroporous and interconnected nature of the cryogel materials can provide a significant advantage as adsorbents in both batch and continuous flow processes. Indeed, while continuous water flow inside the hydrogel is generally slow or not possible, within the cryogel, water can flow continuously throughout the sponge-like polymeric structure opening to their use as a filtration column. **Figure 25c** reports the water flow rate measures. The value represents the amount of water passing through a defined thickness of the cryogel matrix per unit of time (1 hour) at a constant hydrostatic pressure. The first composition shows a significantly lower ability to allow solvent flow compared to the case where the crosslinker content is

increased (5.5 mL h^{-1} of water versus almost 280 mL h^{-1}). According to the literature, a higher crosslinking degree makes the cryogel walls more compact, improving the overall structure stability and thus leading to a greater amount of water able to pass through the cryogel's internal network. [76]. On the other hand, also by changing the main monomer (HEA instead of AAm, third composition) we greatly improve the water flow ability, although slightly lower than the second cryogel (Cryo-A2 with higher crosslinking degree).

3.2.2 Gold adsorption in single metal solution and kinetic model

These cryogel can be used as adsorbents for gold dissolved in acid solution directly, without the need for further chemical treatment, thus offering an advantage for their large-scale application. A detailed analysis of the gold adsorption capacity and kinetics was carried out using aqueous solutions of Au(III) cations, prepared by dissolving $HAuCl_4$ salts in water and adjusting the pH = 1. A specific amount of cryogel was immersed in different concentration solutions and the adsorption process proceeded at room temperature without any stirring/shaking of the solution. The residual gold concentration in solution was monitored using UV-Visible spectroscopy over an extended period, following the same protocol used in a previous study [24]. As an example, **Figure 26a** illustrates an UV-Vis absorbance measurement of a solution before and after the adsorption process.

During the approximately 220-hour adsorption process, UV-Vis absorbance measurements indicate a time-dependent decrease in the absorption peak associated with gold ions (at 314 nm). Using the Lambert-Beer law and the molar extinction coefficient calculated in previous studies [24], the reduction in the concentration of gold ions in the bulk solution is quantified. Simultaneously, a reddish coloration develops mainly in the central region of the adsorbent material

(**Figure 26b**). This color change over time suggests that the material not only adsorbs gold ions from the surrounding solution but also reduces them to their metallic form. The observed coloration can be attributed to plasmonic surface resonance absorption, further supported by SEM analysis, which confirms the presence of gold nanostructures, as shown in **Figure 26c**.

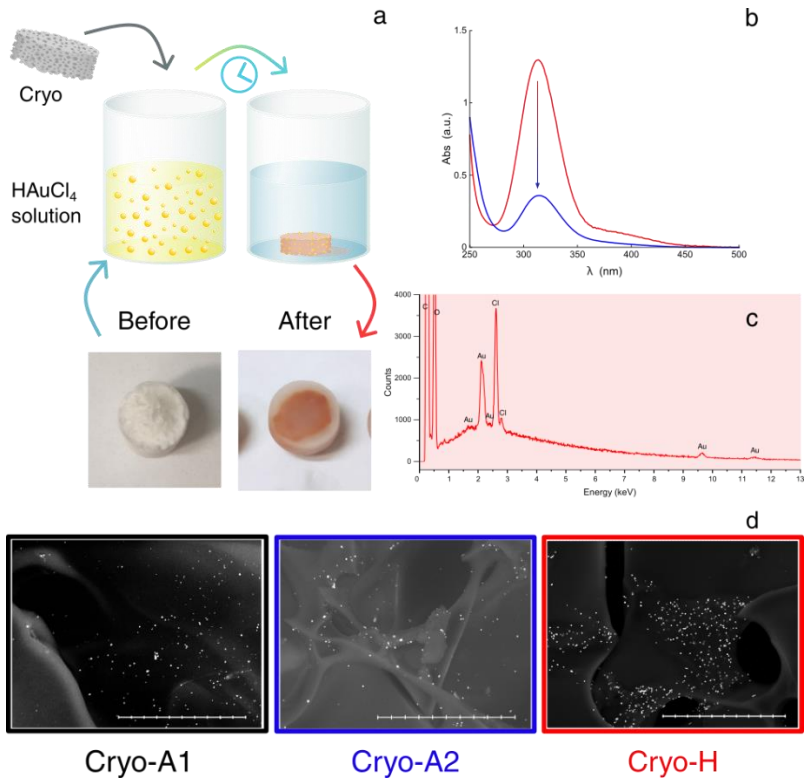

Figure 26. Gold adsorption in single metal ion solutions. Scheme of gold adsorption protocol, together with the visual appearance of one cryogel section before and after immersion in a gold solution (100 mg L^{-1}) (a); Example of UV-Vis spectra of initial metal solution (red) and the same after 1 week of cryogel treatment (blue) (b); EDS measurement of Cryo-H after the immersion in a gold solution (100 mg L^{-1}) for 1 week (c); SEM images of lyophilized cryogels polymeric matrix after the immersion in gold solution; scale bar = 30 μm (d).

In contrast to hydrogels studied in the previous chapter, which often display micrometric gold structures or plates, the structures identified in this material are exclusively nanoscale, with dimensions reaching up to a few hundred nanometers but never extending into the micrometric range. Additional SEM images are provided in **Figure 27**.

Figure 26d shows the EDS measurement, which supports the identification of the bright spots in the SEM images as elemental gold, thanks to the recognition of their characteristic peaks.

To investigate the metal recovery performance as a function of the material chemical composition, the three different cryogels were immersed in different aqueous solutions (with gold at a concentration of 20 mg L^{-1} and 100 mg L^{-1}) for more than 200 hours and the adsorption properties were compared. **Figure 28a** shows the decay of gold concentration as a function of time, starting from the immersion of the cryogel material. While the difference is minimal at the lowest concentration, with similar recovery percentages (77%, 89%, and 91%, respectively), notable differences in adsorption kinetics emerge at the highest concentration tested. At this level, the Cryo-H composition exhibits significantly faster and more efficient kinetics, achieving nearly 20% higher gold recovery compared to the other compositions. Along with the swelling capacity characterizations and its significant advantage over other compositions in the thermogravimetric measurements shown in **Figure 22b**, this characterization highlights the improved performance of the composition containing HEA instead of AAm. Therefore, this material was chosen for more detailed studies on adsorption kinetics. **Figure 28b-c** illustrate the time-dependent trends in gold ion concentration decay and adsorption capacity (Qt) for solutions with concentrations ranging from 20 mg L^{-1} to 100 mg L^{-1}.

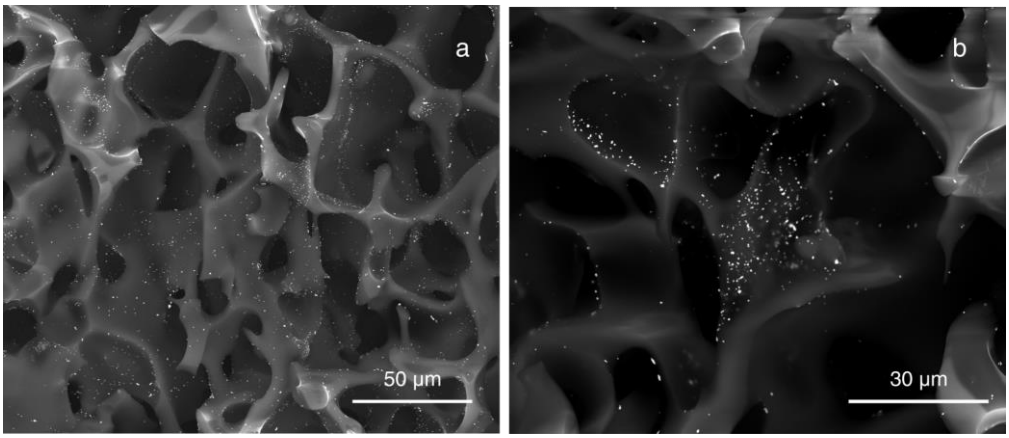

Figure 27. More SEM images of Cryo-H after the immersion in a gold solution (with C_0 = 100 mg L^{-1}). The scale bars are 50 µm (a) and 30 µm (b), respectively.

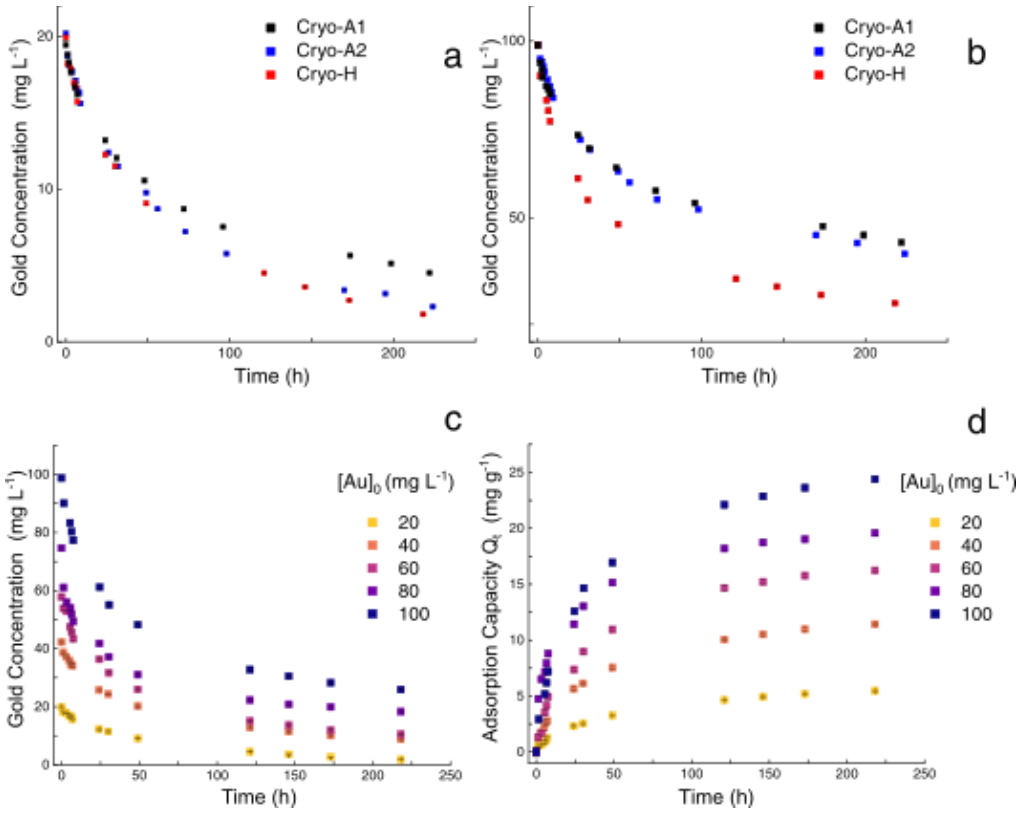

Figure 28. Comparison on cryogel adsorption performance. Residual gold concentration in as a function of cryogel immersion time (h) in solution with a starting

concentration of 20 mg L^{-1} (a) and 100 mg L^{-1}(b); Residual gold concentration (c) and Qt (d), as a function of Cryo-H cryogel immersion time (h) at various starting concentrations of gold ions.

As previously defined in Chapter 2, the most important parameter used in adsorption kinetics studies is the Adsorption Capacity Q_t. The corresponding equation is recalled below:

$$Q_t\,(\text{mg g}^{-1}) = (C_0 - C_t) \cdot V / m \qquad (1)$$

where C_0 (mg L^{-1}) represents the initial concentration of the solution, C_t (mgL^{-1}) is the residual concentration of gold ions measured at time t, V(L) denotes the volume of the treated solution, and m (mg) is the dry mass of the adsorbent material.

The trend of the parameter Q_t (see equation 1) at equilibrium (i.e. Q_e ,corresponding to $Q_{t=218h}$) as a function of starting concentration (C_0), serves as a crucial indicator of the material's maximum adsorption capacity. We can indeed observe that the higher the initial concentration of the solution, the greater the value of Q_e (**Figure 28c**). Even higher Q_e values are observed with increased initial concentrations, reaching 134.7 mg g^{-1} for cryogels containing HEA-AAc at a starting concentration of 800 mg L^{-1}. Additionally, the temporal trend of Q_t is extensively used in the literature to investigate adsorption mechanisms. The adsorption kinetics in these systems are notably complex, involving several dynamic stages linked to distinct mass transport phenomena. A simplified yet effective framework identifies three main steps in the adsorption process for porous materials. First, gold ions diffuse externally through the aqueous layer surrounding the hydrogel, driven by the concentration gradient between the bulk solution and the adsorbent surface. Next, the ions penetrate the hydrogel's pores

via internal diffusion. Finally, they bind to the active sites of the adsorbent [20]. Building on the review by Pasquier and Largitte [71] regarding the models employed in the literature to describe adsorption kinetics, several key approaches stand out as the most frequently applied. Notably, an important distinction has been drawn between models aimed at representing the overall adsorption process and those specifically developed to capture the phenomena of intraparticle diffusion. However, it is evident that these two perspectives are complementary and together provide a more comprehensive understanding of the system. Models for the overall adsorption process, such as the pseudo-first order (PFO) and pseudo-second order (PSO) models, focus on describing the rate at which adsorbed ions or molecules approach equilibrium on the adsorbent surface. On the other hand, intraparticle diffusion (IP) models are more specialized, focusing on the movement of ions within the pores of the adsorbent material. Among these, the Weber and Morris model (IP-WM) has proven particularly effective in describing the adsorption kinetics of metal ions and other pollutants in porous materials.

According to the Intraparticle model (see equation 3), the adsorption process is controlled by only intraparticle diffusion if the plot of Q_t vs $t^{1/2}$ gives a single straight line passing through the origin. Otherwise, if the plot is not a straight line or does not pass through the origin, it suggests that intraparticle diffusion is not the sole mechanism involved. For example, if the intercept (let's say C_{intra}) is not zero, the adsorption process is affected by a boundary layer effect, and the C_{intra} value is related to the thickness of the boundary layer, which reflects the external mass transfer resistance during adsorption. A higher C_{intra} value indicates a more pronounced boundary layer effect. This concept is reinforced by foundational studies like Weber and Morris (1963) and further explored in subsequent research [80,81]. **Figure 28c** reports the non-linear trend

as a function of time for the material adsorption capacity Q_t, while the adsorption kinetics fitted with the IP model are shown in **Figure 29a**.

The values C_{intra} reported in **Table 9,** zero for almost all tested initial gold concentrations. This seems to suggest that the intraparticle diffusion could be proposed as the main mechanism in the overall diffusion and adsorption process. On the other hand, the multilinearity may indicate the involvement of competing mechanisms within the overall process.

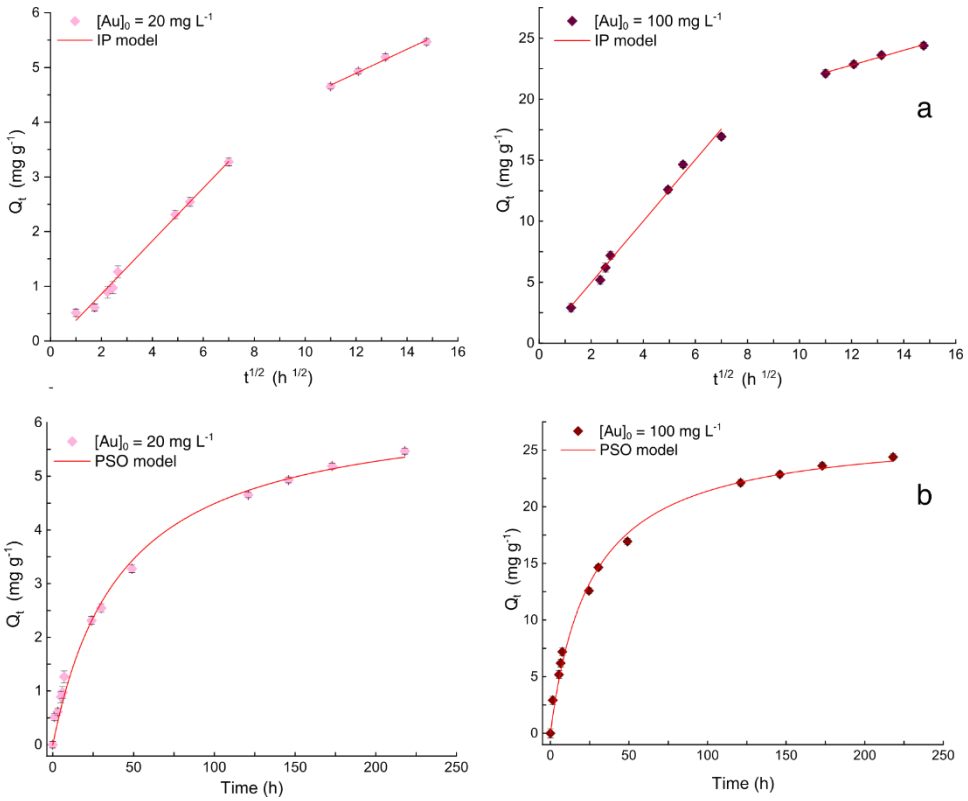

Figure 29. Kinetics Adsorption Intraparticle model and Pseudo-Second Order model. Intraparticle (IP) model (a) and Pseudo-Second Order (PSO) model (b) fitting function relative to the lowest (20 mg L^{-1}, *left*) and highest (100 mg L^{-1}, *right*) starting gold concentration.

Table 9. Fitted Kinetic Parameters Values for **Intraparticle** model. Experimental Conditions: pH=1, V_{sol}=100 mL, Cryo-H dry weight = 300 mg, room temperature (i.e. 25 °C).

C_0 (mg L^{-1})	$k_{intra,1}$ (mg g^{-1} $h^{-1/2}$)	C_{intra} (mg g^{-1})	R^2	$k_{intra,2}$ (g mg^{-1} $h^{-1/2}$)	R^2
20	0.48 ± 0.02	-0.11 ± 0.07	**0.992**	0.22 ± 0.01	**0.990**
40	1.11 ± 0.04	-0.0 ± 0.2	**0.994**	0.37 ± 0.03	**0.986**
60	1.65 ± 0.09	-0.4 ± 0.4	**0.983**	0.42 ± 0.04	**0.981**
80	1.83 ± 0.08	0.8 ± 0.2	**0.988**	0.36 ± 0.03	**0.988**
100	2.5 ± 0.1	-0.1 ± 0.6	**0.988**	0.61 ± 0.04	**0.990**

Table 10. Fitted Kinetic Parameters Values for **Pseudo-second order** model. Experimental Conditions: pH=1, V_{sol}=100 mL, Cryo-H dry weight = 300 mg, room temperature (i.e. 25 °C).

C_0 (mg L^{-1})	Q_{e_exp} (mg g^{-1})	Q_{e_fit} (mg g^{-1})	K_2 (g mg^{-1} h^{-1})	R_{PSO}^2
20	5.47 ± 0.06	6.4 ± 0.2	7.8 ± 0.8	**0.994**
40	11.4 ± 0.1	12.7 ± 0.3	2.6 ± 0.2	**0.993**
60	16.2 ± 0.2	18.3 ± 0.5	1.9 ± 0.2	**0.991**
80	19.6 ± 0.2	20.1± 0.6	1.1 ± 0.1	**0.984**
100	24.4 ± 0.3	26.9 ± 0.5	1.05 ± 0.08	**0.994**

In addition to the IP model fitting the Q_t vs $t^{1/2}$ plot, it can be useful to use complementary kinetic models (e.g., the pseudo-first or pseudo-second-order model) to verify the validity of the proposed mechanism.

The differential forms of the PFO and PSO models have been described by equations 4 and 5 in the previous Chapter.

The adsorption process and interaction between gold ions in solution and Cryo-H were analyzed by fitting the experimental data to Pseudo-First order and Pseudo-Second order kinetic models, using Equation 4.a and 5.a, respectively. Adsorption kinetic models provide insight about whether the adsorption process is physical or chemical. In **Figure 29b** the non-linear form of PSO (see equation 5) model fitting the experimental data are shown, for both the lowest and highest concentration solution. The fitted parameters values for the PSO model are reported in **Table 10**.

The linear regression correlation coefficient ($R_2^2 \cong 0.994$) value from the pseudo-second order model was close to unity and slightly higher than that ($R_1^2 \cong 0.975$) from the pseudo-first order model (reported in **Table 10** and **Table 11**, respectively). Moreover, in **Figure 30** is reported the comparison between the PFO and PSO fitting equation, indicating that the adsorption process matches the pseudo-second order model better than the pseudo-first order, and chemical adsorption, - most likely the gold ions reduction on the polymeric matrix edge - dominates the process.

Table 11: Fitted Kinetic Parameter Values for **Pseudo-First order** model. Experimental Conditions: pH=1, V_{sol}=100 mL, Cryo-H dry weight = 300 mg, room temperature (i.e. 25 °C).

C_0 (mg L^{-1})	Q_{e_exp} (mg g^{-1})	Q_{e_calc} (mg g^{-1})	K_1 (10^{-2} h^{-1})	R_{PFO}^2
20	5.47 ± 0.06	5.2 ± 0.1	2.2 ± 0.2	**0.983**

40	11.4 ± 0.1	10.8 ± 0.3	2.8 ± 0.3	**0.976**
60	16.2 ± 0.2	15.6 ± 0.5	2.8 ± 0.3	**0.975**
80	19.6 ± 0.2	17.8± 0.6	3.5 ± 0.4	**0.952**
100	24.4 ± 0.3	23.3 ± 0.6	3.2 ± 0.3	**0.974**

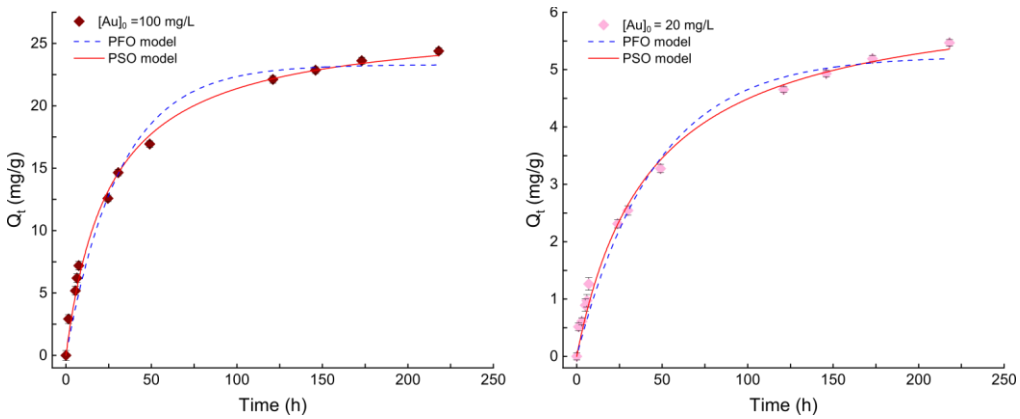

Figure 30. Comparison of Pseudo-First Order (PFO) model (dotted blue line) and Pseudo-Second Order (PSO) model (solid red line) fitting function relative to the highest (100 mg L^{-1}, *left*) and lowest (20 mg L^{-1}, *right*) starting gold concentration.

3.2.3 Separation of gold from other noble metal

This section focuses on the use of the Cryo-H selected composition as an adsorbent material for a mixed noble metal solution. Cabro S.p.A. provided reference conditions to prepare a solution that closely simulates real industrial wastewater. This solution contains metal ions such as Au(III), Pd(II), Pt(IV), Ru(III), Rh(III), and Ir(III), with concentrations not exceeding 20 mg L^{-1} for each metal and an operating pH of 1. A key challenge in treating such solutions lies in achieving selective recovery of a specific metal while minimizing interference

from others. Recent studies on adsorption-based recovery strategies have demonstrated significant gold recovery but lacked selectivity in the presence of platinum group metals.

Under the given working conditions, our cryogel exhibits selectivity for all platinum group metals. The treatment of the mixed metal solution was carried out through a batch test, wherein the cryogel was immersed directly in the solution, and the metal ion content was monitored over time (**Figure 31a**). After one week, a detailed quantification of the metal concentrations following cryogel adsorption is presented in **Figure 31b** - showing an efficient separation of gold from other metals - and the corresponding recovery percentages illustrated in **Figure 31c**. In this analysis, the metal concentrations were determined using Inductively Coupled Plasma Optical Emission Spectrometry (ICP-OES), as the complexity of the solution rendered UV-visible spectroscopy unsuitable. To further characterize selectivity, Energy-Dispersive Spectroscopy (EDS) measurements were conducted. **Figure 31d** shows the EDS spectrum of Cryo-H after one week of immersion in the mixed metal solution. Characteristic gold peaks are clearly visible, along with minimal traces of palladium. Notably, no characteristic peaks for ruthenium were detected, aligning with the selectivity measurements shown in **Figure 31b** and **32.**

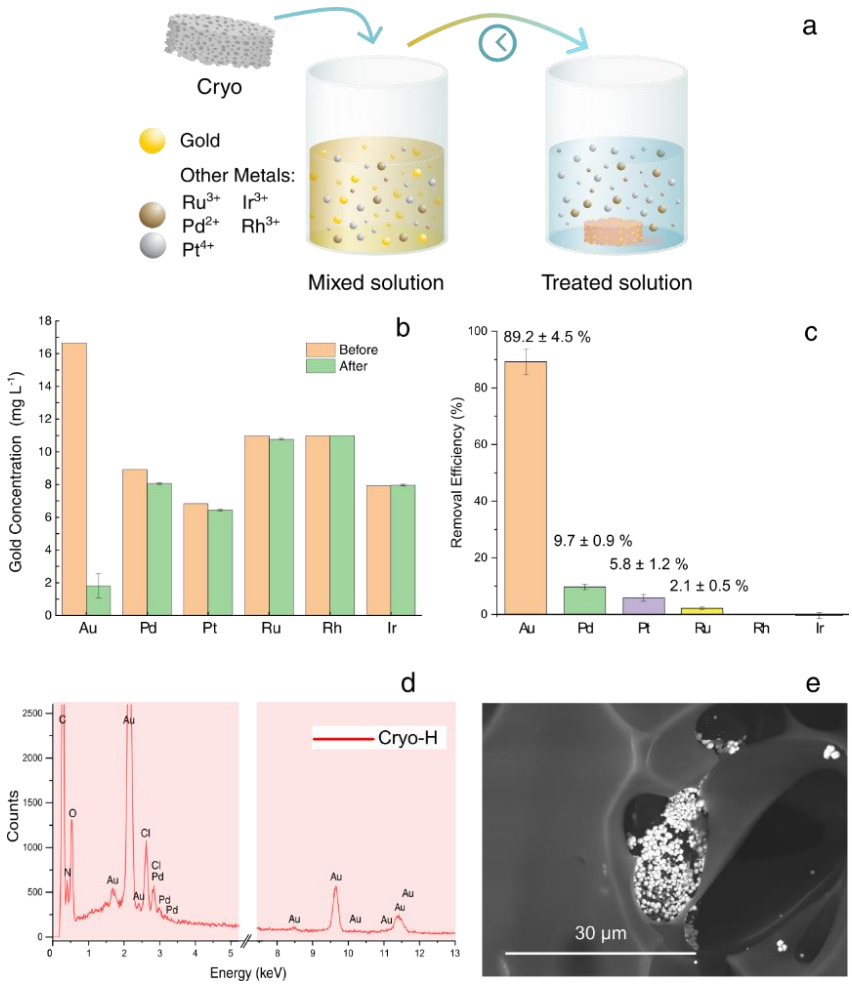

Figure 31. Application and selectivity. Scheme for selective gold separation from industrial wastewater (a); Concentration of different metals in a mixed solution before and after the Cryo-H hydrogel treatment (b); Percentage of metal ions recovery for Cryo-H immersed (1 week) into the mixed metal solution (c); EDS measurements of lyophilized Cryo-H after immersion (1 week) in the multi-metal solutions (d) and the corresponding spot shown by a SEM image demonstrating formation of metallic nanoparticles on the polymeric architecture (e).

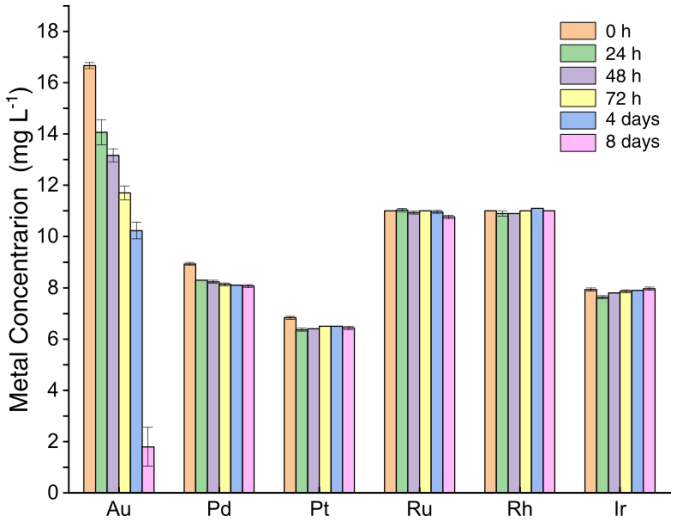

Figure 32. Further insight into gold recovery in a mixed metal solution: Concentration of residual metal ions (mg L^{-1}) in the mixed solution as a function of Cryo-H immersion time. Measurements were conducted using ICP-OES elemental analysis, provided by Cabro S.p.A.

3.3. CONCLUSIONS

In summary, the investigation into the Cryo-H cryogel has demonstrated its remarkable capabilities as an adsorbent material for noble metal recovery from aqueous solutions. The material's high adsorption capacity, rapid kinetics, and selectivity for gold in both single-metal and mixed-metal solutions highlight its potential for industrial applications. In single-metal solutions, the cryogel exhibited efficient gold recovery while facilitating the reduction of gold ions to their metallic form, as confirmed by SEM and EDS analyses.
In mixed noble metal solutions designed to simulate industrial wastewater, Cryo-H showed superior selectivity for gold, with minimal interference from platinum group metals. The cryogel's suitability for selective separation processes is a critical requirement for practical applications in industrial effluent treatment, and it has been validated through ICP-OES and EDS analyses.
These findings allow us to state the material offers the dual advantage of being directly usable as an adsorbent after cryopolymerization, without the need for further chemical or physical treatments. Additionally, it shows promise for thermal degradation to recover pure solid metals, leaving no residue of the polymeric matrix after decomposition. The material also exhibits slightly faster and more efficient kinetics compared to traditional hydrogels with similar monomer compositions, enhancing its practicality for real-world applications.
In conclusion, Cryo-H is highly promising as a scalable and sustainable solution for noble metal recovery, with significant potential to address the challenges of industrial wastewater treatment. Future efforts should aim to optimize its performance under varying operational conditions, evaluate its recyclability over multiple cycles, and explore its application to other high-value metals.

3.4. EXPERIMENTAL SECTION

3.4.1. Materials

Acrylamide (AAm), Acrylic acid (AAc), N,N'-Methylenebisacrylamide (BIS), hydroethylacrylate (HEA), Ammonium PerSulfate (APS), tetramethylethylenediamine (TEMED), tetrachloroauric(III) acid trihydrate ≥ 99.9% ($HAuCl_4 \cdot 3H_2O$), and Hydrochloric acid (HCl) were purchased from Sigma-Aldrich and used as received without further modification. The mixed noble metal waste solution (containing Pt (IV), Rh (III), Ir (III), Pd (II), Ru (III)) has been provided by Cabro S.p.A.

3.4.2. Cryogel materials synthesis

The cryogels were prepared using a monomer solution containing AAm or HEA as the major monomer, AAc as comonomer, and BIS as crosslinker. Monomers and crosslinker different ratios are reported in **Table 7**. To avoid polymerization at room temperature, all solutions have been placed in the fridge for 30 minutes before the addition of APS and TEMED.

Then a 10% m/V solution of APS was added to achieve a final concentration of 0.25% of initiator and - as final step - a 10% m/V solution of TEMED was added to achieve a final concentration of 2.25%, in order to promote the polymerization. After TEMED addition, the tubes were placed in a cryostat (CC-K6 - Huber) at -18°C for 18 hours. After thawing, the cryogels were washed with deionised water and lyophilized.

3.4.3. Chemical-physical materials characterization

The swelling tests were performed both in deionised water and acid solution (1M HCl). The Equilibrium Water Content (EWC) has been determined by gravimetric methods, calculating the ratio of the weight of water contained at the maximum swelling to the weight of the completely swollen cryogel, following the equation:

$$EWC\ (\%) = [\ (m_s - m_d) / m_s\ ] \times 100 \qquad (10)$$

where m_s (g) is the weight of the cryogel in its swollen state, and m_d (g) is the weight of the cryogel in its dried state. The measure was executed by immersing cryogel in both solutions for 1 hour and weighting the cryogel sample swelled. The samples have been placed in a purpose-built metallic cage (see **Figure 33**) and, after immersion, dried for 5 seconds on a paper towel and weighted. For each composition, the measurements were repeated in triplicate and the averaged values are reported in **Table 2**.

Figure 33. An example of how the purpose-built metallic cages look like and how a swelling degree test was conducted.

The water flow rate has been tested also. In this test a hydrostatic pressure of 1 meter of water is exercised on the cryogel material and the result is a measure of

how much water (mL) (values reported in **Table 8)** can pass through the sample in a defined time interval (1h). The sample is placed in the same tube that we used in the cryostat but in the bottom, it has a hole with the diameter of 0.5 cm, so the water can pass through it. As further characterization the chemical composition of cryogels, both before and after the gold loading into a pure and mixed solution, was characterized by a Fourier transform infrared (Spectrum UATR Two, Spectrometer PerkinElmer) spectroscopy (ATR-IR) with a resolution of 1 cm^{-1} over the range 400–4000 cm^{-1}. Other structural characterization measurements were carried out using Scanning Electron Microscopy (SEM): using the FlexSEM 1000 (Hitachi) images of the cryogel both before and after metal ion adsorption and reduction were acquired to examine the internal structure. Moreover, both for pure metal and mixed solutions, the EDS measurements on cryogel matrix have been performed (SEM Inspect-F), confirming the presence of elemental gold on adsorbent material. TGA was performed (SDT Q600 T.A. Instruments, provided by Cabro S.p.A). over a temperature range of 20 to 800°C, with a heating rate of 5°C/min up to 300°C and 10°C/min from 300°C to 800°C, under an air atmosphere.

3.4.4. Gold ions adsorption experiments

Batch adsorption tests were carried out by placing Cryo-AAc-based cryogels, swollen from 300 mg of dry material, into 100 mL solutions with varying initial gold concentrations (20, 40, 60, 80, 100 mg L^{-1}) or a mixture of metal ions. The gold solutions preparation and adsorption experiments followed the procedure already described in Chapter 2 [24]. The measures of residual gold concentration in pure gold solutions were performed by means of UV-Vis Spectroscopy (LAMBDA 950 UV/Vis spectrophotometer, PerkinElmer). The mixed metal cation solution was provided by Cabro S.p.A., prepared under the same conditions as in the previous chapter. The final composition includes

approximately 20 mg L^{-1} of each metal and has a pH of 1. Residual metal cation concentrations were monitored using ICP-OES elemental analysis (5110 ICP-OES, Agilent supplied by Cabro S.p.A).

4. Conclusions

This study demonstrates the exceptional potential of Poly(Acrylamide-co-Acrylic Acid) hydrogels, together with the Acrylic Acid-based Cryogel, as novel adsorbent materials for the efficient recovery of noble metals, especially gold, from aqueous solutions.

The hydrogels, synthesized via free-radical polymerization of acrylamide and acrylic acid, exhibit remarkable adsorption capabilities, good selectivity, and rapid kinetics for gold recovery, even in complex mixed-metal solutions mimicking industrial wastewater. Notably, these materials are capable of spontaneously reducing gold ions to their metallic form, forming particles of varying sizes (from 50 nm nanoparticles to microplates), which are well-dispersed within the polymer matrix, eliminating the need for external reducing agents and minimizing environmental impact.

The Cryo-H cryogel, obtained through a different polymerization process, further demonstrates superior selectivity for gold in mixed-metal systems containing platinum group metals such as palladium, platinum, ruthenium, rhodium, and iridium, which typically compete for adsorption sites. This selectivity is a critical advantage, as the cryogel efficiently separates gold from other metals, with minimal interference from the platinum group metals, especially from ruthenium in comparison with the hydrogel material. Cryogel

material allows a metal separation issue that is difficult to achieve in other ways (especially from Ru, Pd, and Pt in comparison with hydrogel materials) and without any chemical adjustment (e.g., pH or reducing agent addition) of the treated industrial wastewater.

Batch test results confirmed high gold recovery percentages, with low retention of competing metals, as validated through ICP-OES and EDS analyses. The observed selectivity is largely driven by the cryogels reduction mechanism, which is particularly effective under acidic pH conditions, where gold is selectively reduced, and interactions with other metal ions are less favored.

Moreover, Cryo-H offers the dual advantage of being directly usable as an adsorbent after cryopolymerization, without the need for additional chemical or physical treatments, enhancing its practicality for real-world applications. The material also shows promise for thermal degradation to recover pure solid metals, leaving no residue of the polymeric matrix after decomposition, positioning it as a sustainable solution for noble metal recovery. In comparison to traditional hydrogels with similar monomer compositions, Cryo-H exhibits slightly faster and more efficient kinetics, further enhancing its suitability for large-scale, real-world applications.

The outcomes of this effort provide insights into the driving mechanisms behind metal ion adsorption, although, to our knowledge, there is a lack of a comprehensive physical model capable of fully explaining the complex interactions involved in diffusion and adsorption processes.

In conclusion, both hydrogels and cryogels, based on the main monomers such as HEA, acrylamide, and acrylic acid, as investigated in this study, offer scalable, sustainable, and highly effective solutions for the recovery of noble metals,

particularly gold, and provide a promising pathway to address the challenges of industrial wastewater treatment and metal recycling.

Future studies should focus on enhancing and tailoring material selectivity, exploring the ability to adjust selectivity towards even more difficult-to-recover metals, such as ruthenium, and expanding its application to other high-value metals. Furthermore, additional experiments on diffusion models will be carried out in collaboration with Prof. Francesco Piazza from University of Florence, focusing on uncovering the key mechanisms driving the kinetics of these systems, particularly within the framework of a broader project aimed at designing and studying nano-porous materials for wastewater remediation, conceived thanks to the results of this PhD work. The aim is to develop a non-phenomenological theoretical model capable of reproducing the experimental data obtained. This research represents a natural progression of the ongoing work, seeking to elucidate the reasons behind the remarkable performance of these systems and to identify the primary factors that govern their kinetic behaviour.

List of Work:

- Journal Article: P. Cinfrignini, A. Boschetti, G. Ghini, A. Tenti, M. Plazanet, D. Martella, R. Torre; A Gold Rush: Designing Hydrogels for Selective Recovery in Wastewater Containing Mixed Metal Ions, *ACS Applied Materials & Interfaces*, **2024**, *16,49*, DOI: 10.1021/acsami.4c15657.
- Journal Article: P. Cinfrignini, D. Resmini, A. S. Calderon, A. Boschetti, G. Ghini, A. Tenti, F. Celegato, R. Torre, Maria Rosa Aguilar, Daniele Martella; Enhanced recovery of gold from other noble metals using acrylic acid-based cryogel adsorbents, submitted manuscript.
- Research project (submitted): *"Design, synthesis and characterization of next-generation nanostructured materials for wastewater remediation*" (DeSC-Nano), co-financed by the Proposing Institution and by *Ministero degli Affari Esteri e della Cooperazione Internazionale* (MAECI). Status: Under Review. Partners: University of Florence (Italy), Universidade Federal de Pelotas (Brazil).

References:

1. Introduction

[1] https://www.google.com/url?q=https://www.gold.org/goldhub/data/gold-demand-by-country&sa=D&source=docs&ust=1734606939857696&usg=AOvVaw3auHyIcZCHUYlH6ARR8zWj (accessed 2024-09-01)

[2] Ahmed, S., Ahmad, M., & Zhang, J. Environmental and economic assessment of food waste management options: A case study of the UK. *Waste Management,* 2022, *139*, 105–115.

[3] Zupanc, A., Install, J., Jereb, M., & Repo, T., Sustainable and selective modern methods of noble metal recycling. *Angewandte Chemie International Edition*, 2023, 62(5), e202214453.

[4] Zupanc, A., Install, J., Jereb, M., & Repo, T., Trash or treasure? Sustainable noble metal recovery. *Green Chemistry,* 2024, *26*, 5684–5695.

[5] Zhang, C., Gu, Q., Wang, Y., Ye, J., Zhou, Q., Bai, S., Zhang, Z., Luo, J., Xiong, Y., & Zheng, Y. (2022). Iodine-catalysed dissolution of elemental gold in ethanol. *Angewandte Chemie International Edition, 61*(25), e20211758.

[6] Li, J., Ma, Y., Duong, T. T. T., Nguyen, A. V., & Amal, R. (2021). Selective recovery of precious metals through photocatalysis. *Nature Sustainability, 4*(7), 618–626.

[7] Liu, Y., et al. (2013). Selective isolation of gold facilitated by second-sphere coordination with α-cyclodextrin. *Nature Communications, 4*, Article 1855.

[8] B. Xu, Y. Chen, Z. Dong, T. Jiang, B. Zhang, G. Liu, J. Yang, Q. Li, Y. Yang, Eco-friendly and Efficient Extraction of Valuable Elements from Copper Anode Mud Using an Integrated Pyro-hydrometallurgical Process. *Resources, Conservation & Recycling*, vol. 164, 2021, 105195.

[9] Wang, J., Zhang, Z., Xu, X., & Xu, Z. (2019). Evaluation of simple amides in the selective recovery of gold from secondary sources by solvent extraction. *ACS Sustainable Chemistry & Engineering, 7*(15), 15019–15029.

[10] Li, J., Li, M., & Xie, J. (2022). Review: Adsorbents for the recovery of precious metals from wastewater. *Journal of Materials Science, 57*(18), 10886–10911.

[11] Zhao, H., & Li, H. (2014). Biosorbents for recovery of precious metals. *Bioresource Technology, 160*, 203–212.

[12] M. Peydayesh, E. Boschi, F. Donat, R. Mezzenga, Gold Recovery from E-Waste by Food-Waste Amyloid Aerogels. *Adv. Mater.* 2024, 36, 2310642.

[13] S. Chen, J. Wu, Z. Yang, J., D. Bhattacharyya, H. Wan, W. Xu, K. Tang, Selective recovery of noble metals from electronic waste leachates via coral-like adsorbents*, Separation and Purification Technology, 2025,* 354, 4.

[14] W. Xu, F. Wang, S. Chen, K. Zhang, K. Tang, Efficient and selective recovery of gold and palladium by simple and easily synthesized polyethylenimine based polymer, *Separation and Purification Technology*, 2024, 328, 125039.

[15] Li, X., Wang, YL., Wen, J. *et al.* Porous organic polycarbene nanotrap for efficient and selective gold stripping from electronic waste. *Nat Commun* , 2023, 14, 263.

[16] Q. Pu, Z. Su, Z. Hu, X. Chang, M. Yang, 2-Mercaptobenzothiazole-bonded silica gel as selective adsorbent for preconcentration of gold, platinum and palladium prior to their simultaneous inductively coupled plasma optical emission spectrometric determination, *J. Anal. At. Spectrom*., 1998, 13, 4, 249-253.

[17] H. Ebrahimzadeh, N. Tavassoli, M.M. Amini, Y. Fazaeli, H. Abedi, Determination of very low levels of gold and palladium in wastewater and soil samples by atomic absorption after preconcentration on modified MCM-48 and MCM-41 silica, *Talanta,* 2010, 81, 4–5, 1183-1188.

[18] K. Fujiwara, A. Ramesh, T. Maki, H. Hasegawa, K. Ueda, Adsorption of platinum (IV), palladium (II) and gold (III) from aqueous solutions onto l-lysine modified crosslinked chitosan resin, *Journal of Hazardous Materials*, 2007, 146, 1 39-50.

[19] A. Haleem, Y. Pan, F. Wu, M. Ullah, S. Chen, H. Li, J. Pan, A customized 3D bio-macroporous cryogels for efficient and selective gold extraction, *Separation and Purification Technology*, 2024, 345, 127305.

[20] F. Yang, Z. Yan, J. Zhao, S. Miao, D. Wang, P. Yang, Rapid capture of trace precious metals by amyloid-like protein membrane with high adsorption capacity and selectivity, *J. Mater. Chem.* A, 2020, 8, 6.

[21] S. Syed, Recovery of gold from secondary sources—A review, Hydrometallurgy, 2012, 115-116.

[22] Barman, M.K., Bhattarai, A. and Saha, B., Applications of ion exchange resins in environmental remediation. (2023), *VJCH,* 61: 533-550.

[23] S. Bolisetty, M. Peydayesh, R. Mezzenga, Sustainable technologies for water purification from heavy metals: review and analysis, *Chem. Soc. Rev.*, 2019, 48, 2.

[24] P. Cinfrignini, A. Boschetti, G. Ghini, A. Tenti, M. Plazanet, D. Martella, R. torre, A Gold Rush: Designing Hydrogels for Selective Recovery in Wastewater Containing Mixed Metal Ions, *ACS Applied Materials & Interfaces*, 2024, 16, 49.

[25] A. Baimenov, D.A. Berillo, S.G. Poulopoulos, V.J. Inglezakis, A review of cryogels synthesis, characterization and applications on the removal of heavy metals from aqueous solutions. *Adv Colloid Interface Sci*. 2020, 276, 102088.

2. Poly(Acrylamide-co-Acrylic Acid) hydrogel as gold adsorbents

[26] F. Ullah, M. B. Hafi Othman, F. Javed, Z. Ahmad, H. Md. Akil, Classification, processing and application of hydrogels: A review, *Materials Science and Engineering: C*, 2015, 57, 414-433, https://doi.org/10.1016/j.msec.2015.07.053

[27] https://www.statista.com/statistics/299609/gold-demand-by-industry-sector-share/ (accessed 2024-09-01)

[28] S. Rengaraj, Kyeong-Ho Yeon, Seung-Hyeon Moon, Removal of chromium from water and wastewater by ion exchange resins, *Journal of Hazardous Materials*, 2001, 87, 1.

[29] Van Deventer J., New Developments in Ion Exchange Resins for the Recovery of Gold in Complex Ores, *Hydrometallurgy,* 2014, 1, 677

[30] M. E. Hassan Ahamed, A. F. Mulaba Bafubiandi, L. Marjanovic, X. Mbianda, Recovery of gold from mining solutions using Au(III)-imprinted

polymeric resins with pyridine, ethylenediamine and aminothiophosphate functionalities, *Mineral Processing and Extractive Metallurgy,* 2019, 128.

[31] Dai Y., Zheng K., Tan Y., Xiang W., Xianyu B., Xu H., Fischesserite-Inspired Recyclable Se-Polyurethanes for Selective Gold Extraction. *Adv. Sustainable Syst.* 2020, 4, 2000072.

[32] W. Liu, L. O. Jones, H. Wu, C.L. Stern, R.A. Sponenburg, G.C. Schatz, J.F. Stoddart, Supramolecular Gold Stripping from Activated Carbon Using α-Cyclodextrin, *J. Am. Chem. Soc*, 2021, 143, 4.

[33] H. Wu, Y. Wang, C. Tang, L.O. Jones, B. Song, X.Y. Chen, L. Zhang, Y. Wu, C.L. Stern, G.C. Schatz, W. Liu, J.F. Stoddart, High-efficiency gold recovery by additive-induced supramolecular polymerization of β-cyclodextrin., *Nat Commun*, 2023, 14, 1284.

[34] Y. Xiang, Y. Liu, M. Li, W. Bai, G. Liu, L. Xu, The recovery of Au(III) by hydrogel-like beads, *Hydrometallurgy,* 2023, 215.

[35] A.G. Kılıç, S. Malcı, O. Çelikbıçak, N. Şahiner, B. Salih, Gold recovery onto poly(acrylamide-allylthiourea) hydrogels synthesized by treating with gamma radiation, *Analytica Chimica Acta*, 2005, 547 (1), 18-25.

[36] E.E. Khozemy, S.M. Nasef, T.M. Mohamed, Radiation Synthesis of Superabsorbent Hydrogel (Wheat Flour/Acrylamide) for Removal of Mercury and Lead Ions from Waste Solutions, *J Inorg Organomet Polym*, 2020, 30, 1669–1685.

[37] M. Peydayesh, R. Mezzenga, Protein nanofibrils for next generation sustainable water purification. *Nat Commun*, 2021, 12, 3248.

[38] S. Bolisetty, R. Mezzenga, Amyloid–carbon hybrid membranes for universal water purification. *Nature Nanotech,* 2016, 11, 365.

[39] M. Peydayesh, E. Boschi, F. Donat, R. Mezzenga, Gold Recovery from E-Waste by Food-Waste Amyloid Aerogels, *Adv. Mater.* 2024, 36, 2310642.

[40] D. Parajuli, H. Kawakita, K. Inoue, K. Ohto, K. Kajiyama, Persimmon Peel Gel for the Selective Recovery of Gold. *Hydrometallurgy,* 2007, 87, 133.

[41] D. Yu, S. Morisada, H. Kawakita, K. Sakaguchi, S. Osada, K. Ohto, K. Inoue, Xi- Ming Song, G. Zhang, R. R. Sathuluri, Gold recovery from precious metals in acidic media by using human hair waste as a new pretreatment-free green material, *Journal of Environmental Chemical Engineering*, 2021, 9.

[42] Q. Lv, Y. Shen, Y. Qiu, M. Wu, L. Wang, Poly (acrylic acid)/poly(acrylamide) hydrogel adsorbent for removing methylene blue, *J Appl Polym Sci*., 2020, 137, 43.

[43] Y. Wang, L. Zeng, X. Ren, H. Song, A. Wang, Removal of Methyl Violet from aqueous solutions using poly (acrylic acid-co-acrylamide)/attapulgite composite, *Journal of Environmental Sciences*, 2010, 22, 7-14.

[44] D. Li, W. Zhan, W. Zuo, L. Li, J. Zhang, G. Cai, Y. Tian, Elastic, tough and switchable swelling hydrogels with high entanglements and low crosslinks for water remediation, *Chemical Engineering Journal*, 2022, 450, 4.

[45] E. Orozco-Guareño, F. Santiago-Gutiérrez, J.L. Morán-Quiroz, S.L. Hernandez-Olmos, V. Soto, W. de la Cruz, R. Manríquez, S. Gomez-Salazar, Removal of Cu (II) ions from aqueous streams using poly(acrylic acid-co-acrylamide) hydrogels, *Journal of Colloid and Interface Science*, 2010, 349, 2.

[46] N. Chowdhury, C.K. Roy, S.H. Firoz, T. Foyez, A.B. Imran, Role of Ionic Moieties in Hydrogel Networks to Remove Heavy Metal Ions from Water, *ACS Omega*, 2021, 6 (1), 836-844.

[47] M. Zendehdel, A. Barati, H. Alikhani, Removal of heavy metals from aqueous solution by poly(acrylamide-co-acrylic acid) modified with porous materials. *Polym. Bull*., 2019, 67, 343–360.

[48] B. Zhao, H. Jiang, Z. Lin, S. Xu, J. Xie, A. Zhang, Preparation of acrylamide/acrylic acid cellulose hydrogels for the adsorption of heavy metal ions, *Carbohydrate Polymer*s, 2019, 224.

[49] J. Bai, Y. Li, J. Du, S. Wang, J. Zheng, Q. Yang, X. Chen, One-pot synthesis of polyacrylamide-gold nanocomposite, *Materials Chemistry and Physics*, 2007, 106.

[50] V.V. Tatarchuk, Y.O. Dobrolyubova, I.A. Druzhinina, V.I. Zaikovskii, P.N. Gevko, E.A. Maksimovskii, S.A. Gromilov, Facile synthesis of gold nanoparticles in aqueous acrylamide solution., *Russ. J. Inorg. Chem*., 2016, 61.

[51] V. Tatarchuk, S. Gromilov, P. Plyusnin, One-step synthesis and characterization of gold nanoparticles doped polyacrylamide hydrogels. *J Sol-Gel Sci Technol*, 2024, 110.

[52] Y. Song, Z. Li, L. Wang, Y. Yao, C. Chen, K. Cui, One-step preparation of hybrid materials of polyacrylamide networks and gold nanoparticles, *Microsc. Res. Tech*., 2008, 71, 409-412.

[53] D. Shabeeb, A. Haider, A.T. Mohammed, Synthesis of gold nanoparticles using Poly Acrylic Acid as reducing agent – Characterization and in vitro study of anticancer cervix (HELA) activity, *BEST: IJHAMS*, 2017, 4, ISSN (P): 2348-0521, ISSN (E): 2454-4728.

[54] M. Vassallo, M. Vicentini, M. Salzano De Luna, G. Barrera, P. Tiberto, A. Manzin, D. Martella, Magnetic Hyperthermia to Promote Acrylamide Radical Polymerizations, *ACS Applied Polymer Materials*, 2024, 6, 4696-4707.

[55] A. Cappitti, F. Palmieri, R. Garella, A. Tani, F. Chellini, M. Salzano De Luna, C. Parmeggiani, R. Squecco, D. Martella, C. Sassoli, Development of accessible platforms to promote myofibroblast differentiation by playing on hydrogel scaffold composition, *Biomaterials Advances*, 2023, 155.

[56] S. Nesrinne, A. Djamel, Synthesis, characterization and rheological behavior of pH sensitive poly(acrylamide-co-acrylic acid) hydrogels*, Arabian Journal of Chemistry,* 2017, 10.

[57] A. Thakur, R. Wanchoo, P. Singh, Structural Parameters and Swelling Behavior of pH Sensitive Poly(acrylamide-co-acrylic acid) Hydrogels, *Chem. Biochem. Eng. Q.*, 2011, 25 (2).

[58] W. Li, H. Zhao, P.R. Teasdale, R. John, S. Zhang, Synthesis and characterisation of a polyacrylamide–polyacrylic acid copolymer hydrogel for environmental analysis of Cu and Cd, *Reactive and Functional Polymers*, 2002, 52, 31-41.

[59] A.L. Chau, P.T. Getty, A.R. Rhode, C.M. Bates, C.J. Hawker, A.A. Pitenis, Superlubricity of pH-responsive hydrogels in extreme environments, *Front. Chem*., 2022, 10, 891519.

[60] J.A. Peck, C.D. Tait, B.I. Swanson, G.E. Brown, Speciation of aqueous gold (III) chlorides from ultraviolet/visible absorption and Raman/resonance Raman spectroscopies, *Geochimica et Cosmochimica Acta*, 1991, 55 (3), 671-676.

[61] M. Wojnicki, E. Rudnik, M. Luty-Błocho, K. Pacławski, K. Fitzner, Kinetic studies of gold (III) chloride complex reduction and solid phase precipitation in acidic aqueous system using dimethylamine borane as reducing agent, *Hydrometallurgy*, 2012, 127-128.

[62] Y. Naganeyama, T. Tsuruta, Removal, Recovery and Recycle of Gold (III) from Aqueous Solution Using Persimmon Tannin Gel, *International Journal of Geosciences*, 2021, 12 (12), 1084-1094.

[63] J. Wang, X. Guo, Adsorption kinetic models: Physical meanings, applications, and solving methods, *Journal of Hazardous Materials*, 2020, 390, 122156.

[64] J. Wang, X. Guo, Rethinking of the intraparticle diffusion adsorption kinetics model: Interpretation, solving methods and applications, *Chemosphere*, 2022, 309, 136732.

[65] B. Obradović, Guidelines for general adsorption kinetics modeling, *Hemijska industrija*, 2020, 74, 65-70.

[66] S. Tang, L. Lin, X. Wang, A. Feng, A. Yu, Pb(II) uptake onto nylon microplastics: Interaction mechanism and adsorption performance, *Journal of Hazardous Materials*, 2020, 386, 121960.

[67] P. R. Sera, P. N. Diagboya, S. O. Akpotu, F. M. Mtunzi, T. B. Chokwe, Potential of valourized Moringa oleifera seed waste modified with activated carbon for toxic metals decontamination in conventional water treatment, *Bioresource Technology Reports*, 2021, 16, 100881.

[68] S. Lagergren, Zur theorie der sogenannten adsorption geloster stoffe, Kungliga Svenska Vetenskapsakademiens. *Handlingar,* 1898, 24, 1-39.

[69] Y.S. Ho, G. McKay, Pseudo-second order model for sorption processes. *Process Biochemistry*, 1999, 34(5), 451-465.

[70] S. Azizian, Kinetic models of sorption: a theoretical analysis. *Journal of Colloid and Interface Science*, 2004, 276(1), 47-52.

[71] L. Largitte, R. Pasquier, A review of the kinetics adsorption models and their application to the adsorption of lead by an activated carbon, *Chemical Engineering Research and Design*, 2016, 109, 495-504.

[72] M. M. Taqui Khan, G. Ramachandraiah, A. Prakash Rao, Ruthenium (III) Chloride in Aqueous Solution: Electrochemical and Spectral Studies, *Inorg. Chem.,* 1986, 25, 665-670.

[73] L. Panariello, S. Damilos, H. du Toit, G. Wu, A.N.P. Radhakrishnan, I.P. Parkin, A. Gavriilidis, Highly reproducible, high-yield flow synthesis of gold nanoparticles based on a rational reactor design exploiting the reduction of passivated Au(iii), *React. Chem. Eng*., 2020, 5, 663-676.

3. Cryogels: a novel porous material for gold scavenging from wastewater

[74] A. Baimenov, D.A. Berillo, S.G. Poulopoulos, V.J. Inglezakis, A review of cryogels synthesis, characterization and applications on the removal of heavy metals from aqueous solutions. *Advances in Colloid and Interface Science*, 2020, 276, 102088.

[75] D. Türkmen, M. Bakhshpour, S. Akgönüllü, S. Aşır, A. Denizli, Heavy Metal Ions Removal From Wastewater Using Cryogels: A Review. *Front. Sustain.* 2020, 3, 765592.

[76] F. M. Plieva, M. Karlsson, M.R. Aguilar, D. Gomez, S. Mikhalovsky, I. Y. Galaev', Pore structure in supermacroporous polyacrylamide based cryogels, *Soft Matter*, 2005, 1, 4, 303-309.

[77] F. M. Plieva, M. Karlsson, M.R. Aguilar, D. Gomez, S. Mikhalovsky, I.Y. Galaev, Pore structure of macroporous monolithic cryogels prepared from poly(vinyl alcohol). *Journal of Applied Polymer Science*, 2006, 100(2), 1057-1066.

[78] M. Mejia, E. Murillo, Study of the structural, thermal, rheological and film properties of functional copolymers of hydroxyethyl acrylate and methyl methacrylate, *Polìmeros*, 2016, 26(3).

[79] L. Feng, H. Yang, X. Dong, H. Lei, D. Chen, pH-sensitive polymeric particles as smart carriers for rebar inhibitors delivery in alkaline condition. *J. Appl. Polym. Sci*, 2017, 135, 45886.

[80] W.J. Weber, J. C. Morris, Kinetics of adsorption on carbon from solutions. *Journal of the Sanitary Engineering Division*, 1963, 89(2), 31-39.

[81] Y.-C. Wu, Y. -H. Wei, H.-S. Wu, Adsorption and Desorption Behavior of Ectoine Using Dowex® HCR-S Ion-Exchange Resin. *Processes*, 2021, 9(11), 2068.

Acknowledgements

At the end of this enriching and challenging doctoral journey, I would like to express my deepest gratitude to all those who have supported and guided me throughout the realization of this work.

First, I extend my sincere thanks to my supervisor, Prof. Renato Torre, for giving me the opportunity to be part of his research group during these three years of personal and professional growth. I am also grateful to Dr. Alice Boschetti, Dr. Andrea Taschin, Dr. Paolo Bartolini, and Luigi Caminiti for their valuable support and collaboration.

A special thank you goes to Dr. Daniele Martella for his constant guidance, dedication, and professionalism throughout this journey. His expertise and encouragement have been relevant in the realization of this work.

I am also deeply grateful to Prof. Marie Plazanet for hosting me in her research laboratory in Grenoble and for giving me the opportunity to spend six months abroad—an experience that has been academically and personally enriching, providing me with the confidence and motivation I needed. I sincerely thank her for her kindness, expertise, and constant presence, which I had the opportunity to witness and appreciate during my time abroad.

Finally, I would like to thank my family, friends, and colleagues for their support and for always being there for me.

Florence,
April 10th, 2025